

This is an Open Access document downloaded from ORCA, Cardiff University's institutional repository: <https://orca.cardiff.ac.uk/id/eprint/145887/>

This is the author's version of a work that was submitted to / accepted for publication.

Citation for final published version:

Pereira, Ricardo, Mata, João, Ramalho, Ricardo S., Rosas, Filipe M., Silva, Beatriz, Represas, Patrícia and Escada, Cláudia 2022. Nature, timing and magnitude of buried Late Cretaceous magmatism on the central West Iberian Margin. *Basin Research* 34 (2) , pp. 771-796. 10.1111/bre.12640

Publishers page: <http://dx.doi.org/10.1111/bre.12640>

Please note:

Changes made as a result of publishing processes such as copy-editing, formatting and page numbers may not be reflected in this version. For the definitive version of this publication, please refer to the published source. You are advised to consult the publisher's version if you wish to cite this paper.

This version is being made available in accordance with publisher policies. See <http://orca.cf.ac.uk/policies.html> for usage policies. Copyright and moral rights for publications made available in ORCA are retained by the copyright holders.



Nature, timing and magnitude of buried Late Cretaceous magmatism on the central West Iberian Margin

Ricardo Pereira ^{1,2*}, João Mata ², Ricardo S. Ramalho ^{3,2,4,5}, Filipe M. Rosas ², Beatriz Silva ⁶, Patrícia Represas ⁷, Cláudia Escada ⁸

¹ Partex Oil and Gas. Rua Ivone Silva, 6, 1st floor. 1050-124 Lisbon, Portugal.

*Corresponding author. ricardo.pereira@partex-oilgas.com

² Instituto Dom Luiz (IDL), Faculdade de Ciências da Universidade de Lisboa, Campo Grande, 1749-016 Lisbon, Portugal.

³ School of Earth and Environmental Sciences, Cardiff University, Park Place, Cardiff, CF10 3AT, UK.

⁴ School of Earth Sciences, University of Bristol, Wills Memorial Building, Queen's Road, Bristol BS8 1RJ, UK

⁵ Lamont-Doherty Earth Observatory, Columbia University, Comer Geochemistry Building, PO Box 1000, Palisades, NY10964-8000, USA.

⁶ Departamento de Geologia, Universidade de Lisboa, 1749-016, Lisbon, Portugal

⁷ Laboratório Nacional de Energia e Geologia (LNEG), Estrada da Portela, 2610-999 Amadora, Portugal.

⁸ Departamento de Engenharia Geográfica, Geofísica e Energia, Faculdade de Ciências, Universidade de Lisboa, Campo Grande, 1749-016, Lisbon, Portugal

Keywords: Late Cretaceous alkaline magmatism, West Iberian Margin, Fontanelas volcano, sills, lava flows.

Abstract

The magma-poor West Iberian Margin, as part of the Peri-Atlantic alkaline province, records multiple evidence for intra-plate post-rift magmatism. Based on high-resolution multichannel seismic data, this work discusses the presence of large volcanic and intrusive features in the Estremadura Spur, providing evidence for important magmatic activity during the drifting of the continental margin. Our observations reveal distinct voluminous fissure-fed effusive sequences and the details of the 2800 m-high Fontanelas compound volcano, including its external and internal architecture, secondary vents and associated lava flows, all of which were probably extruded at intermediate water depths. Numerous and morphologically diverse sills and sill complexes are also described, attesting to the presence of a Late

37 Cretaceous shallow magmatic plumbing system in the area. Magmatism in this region is
38 interpreted as having occurred during two main pulses and types of activity: 1) Coniacian to
39 lower Campanian(?) age, characterized by fissural and fault-controlled volcanism, which
40 mostly extruded massive lobate/sheet lava flows; and 2) a second voluminous intrusive and
41 extrusive event of mid to late Campanian age, which includes the intrusion of the Estremadura
42 Spur laccolith and the prominent Fontanelas compound volcano with associated dendritic lava
43 flows. The inferred volumes of the first fissure-fed effusive event suggest a large eruption
44 magnitude, comparable to some of the largest historical effusive eruptions. The second
45 magmatic pulse led to the emplacement of discrete clusters of sills and sill complexes, as well
46 as the construction of the ~2.8 km-high Fontanelas volcano, suggesting a syn-rift structural
47 inheritance that controlled the location of the Estremadura Spur Intrusion and the Fontanelas
48 volcanic area. Altogether, a total volume of rock exceeding 1.452 km³ is estimated to have
49 been emplaced or extruded in this region in a relatively short period, attesting to the
50 prominence of the magmatism in this sector of the West Iberian Margin.

51 1. INTRODUCTION

52 Rifting events are often associated with magmatism, which either induced the stretching
53 process by Rayleigh-Taylor instability of the sub-lithospheric mantle (active rifting) or resulted
54 from adiabatic decompression consequence of far-field-induced lithosphere extension
55 (passive rifting) (e.g. Huisman *et al.*, 2001; Geoffroy, 2005). On rifted continental margins,
56 either rich or poor in their magma input, the role of magmatic events are consistently
57 acknowledged to influence to different degrees, the margin's thermal state, eventually leading
58 to breakup and subsequent rebound (e.g. Pérez-Gussinyé *et al.*, 2006; Leroy *et al.*, 2008;
59 Franke, 2013). Additionally, magmatism can also affect fluid flow or the maturation and extent
60 of any potential petroleum systems (e.g. Smallwood and Maresh, 2002; Bischoff *et al.*, 2017;
61 Senger *et al.*, 2017; Mark *et al.*, 2018; Jackson *et al.*, 2020).

62 Lately, developments in the investigation of ancient magmatism on passive continental
63 margins worldwide, with examples from the North Sea (Planke *et al.*, 2017; Walker *et al.*,
64 2020), New Zealand (Bischoff *et al.*, 2019), northwest and south Australia (Magee *et al.*, 2013;
65 Magee *et al.*, 2017), and the South China Sea (Sun *et al.*, 2019), have revealed multiple
66 records of buried volcanism and their associated plumbing systems. Such occurrences are
67 thus recognized as usual characteristic of magma-rich rifted margins, in which plumbing
68 systems are often linked to the period leading to lithospheric rupture and the onset of seafloor
69 spreading, although occasionally persisting up to 10 Ma after breakup (e.g. Jackson *et al.*,
70 2013; Zhao *et al.*, 2016; Planke *et al.*, 2017).

71 The magma-poor and hyper-extended continental margin of West Iberian (Fig. 1), located
72 in the transition from the central to northern Atlantic provinces, exhibits evidence for three

73 distinct magmatic cycles, in which the first two (at ca. 200 Ma and 148-140 Ma, respectively)
74 are associated with two important extensional events during the rifting period and a third post-
75 rift cycle of Late Cretaceous age of more uncertain origin (Manatschal, 2004; Martins *et al.*,
76 2008; Bronner *et al.*, 2011; Mata *et al.*, 2015).

77 This latter cycle postdates lithospheric breakup by ~ 30 Ma., being thus an example of
78 intra-plate post-rift magmatism on the extended continental margin. Magmatic occurrences
79 are well documented onshore (Fig. 2), including Upper Cretaceous magmatism widely
80 distributed in central and south Portugal (Alves, 1964; Wright, 1969; Sparks and Wadge, 1975;
81 Aires-Barros, 1979; Alves *et al.*, 1980; Rock, 1982; Bernard-Griffiths *et al.*, 1997; Miranda *et*
82 *al.*, 2009; Grange *et al.*, 2010) (Fig. 1). In the Estremadura Spur several other offshore
83 occurrences of intrusive and extrusive magmatic rocks has been described or suggested by
84 geophysical potential field methods (Silva *et al.*, 2000; Neres *et al.*, 2018; Escada *et al.*, 2019),
85 as well as by seismic studies, which unveiled a sizeable intrusion assigned to this same
86 (Pereira *et al.*, 2017; Pereira and Barreto, 2018; Pereira *et al.*, 2021). Dredges on the offshore
87 Fontanelas volcano revealed that the characteristics are akin of those depicted by the onshore
88 late Cretaceous magmatism in the neighbouring Lisbon region (Miranda *et al.*, 2010). This
89 magmatic cycle on the West Iberian Margin (WIM) is part of a vast intra-plate magmatic
90 alkaline province that spreads out from the continental margin towards the oceanic domain, in
91 which multiple other intrusions and volcanic buildings have been identified (Matton and
92 Jébrak, 2009; Grange *et al.*, 2010; Merle *et al.*, 2018; Merle *et al.*, 2019). However, even on
93 the neighbouring of the Iberia coastline, the offshore extension of this magmatism, their exact
94 geometry, distribution and origin are still unclear, hampering our complete scientific
95 understanding of the geodynamic evolution and its integration within the overall context the
96 Atlantic.

97 This work primarily provides new insights on the post-rift magmatism affecting the offshore
98 central WIM during the Late Cretaceous, by investigating high-resolution 2D and 3D seismic
99 datasets (Fig. 1). This allowed an accurate morphological characterization of the magmatic
100 features in the area, including evidence for vigorous volcanic and widespread intrusive activity.
101 Critically, this study reveals new data for the Fontanelas volcanic edifice, providing a crisper
102 image of its shallow plumbing systems and extrusive flows. This paper also aims to address
103 the following key scientific questions: 1) What is the nature of the magmatic activity on the
104 offshore WIM? 2) How many magmatic events can be recognised? and 3) What is the
105 magnitude of this event?

106 **2. GEOLOGICAL SETTING**

107 The WIM, developed during the stretching events leading to the opening of the Atlantic
108 Ocean, is one of the most well described hyper-extended passive margins in the world and

109 constitutes a type-example of a magma-poor domain (e.g. Manatschal, 2004; Pérez-Gussinyé
110 *et al.*, 2006; Franke, 2013). Despite the limited magmatic input, magmatism on the WIM is
111 recorded in three main events separated by circa 50 Ma, each associated with distinct phases
112 of the evolution of the Iberian-Newfoundland conjugate margin (e.g. Mata *et al.*, 2015 and
113 references therein): I) the latest Triassic to earliest Jurassic event (Verati *et al.*, 2007), which
114 is part of the Central Atlantic Magmatic Province, exhibiting tholeiitic characteristics, negative
115 ϵNd_i and radiogenic (>0.7050) initial Sr isotope ratios (Martins *et al.*, 2008; Callegaro *et al.*,
116 2014); II) Tithonian-Berriasian (148-140 Ma; Grange *et al.*, 2008; Mata *et al.*, 2015) rift-related
117 mildly alkaline dykes with $+1.6 < \epsilon\text{Nd}_i < +4.2$ and initial Sr isotope ratios close to the CHUR_{145} ;
118 and III) a post-rift alkaline cycle of Late Cretaceous age (98-69 Ma) (Fig. 2), exhibiting $\epsilon\text{Nd}_i >$
119 $+5$ and initial Sr isotope ratios assigned to a sub-lithospheric mantle source with a time-
120 integrated evolution characterized Rb/Sr ratios noticeably lower than the CHUR (Miranda *et al.*
121 *et al.*, 2009; Grange *et al.*, 2010). With time, magmas become more enriched in incompatible
122 elements, whilst their sources were progressively characterized by a lower $^{87}\text{Sr}/^{86}\text{Sr}$ but higher
123 $^{143}\text{Nd}/^{144}\text{Nd}$ ratios and presenting elemental characteristics indicative of increasing depth of
124 magma segregation (Mata *et al.*, 2015). The post-rift cycle has geochemical characteristics
125 compatible with a sub-lithospheric source, with the influence of a plume having been invoked
126 (Grange *et al.*, 2010; Merle *et al.*, 2019). Such plume (*s.l.*) was recently considered as one of
127 the mantle's upwellings zones anchored at the Central East Atlantic Anomaly, ponded below
128 the 660 km anomaly (Civiero *et al.*, 2021).

129 This third cycle is the most significant and widespread magmatic event on the Iberian
130 margin (Fig. 1), testified by multiple exposed manifestations of extrusive and intrusive activity,
131 on the Central and Southern parts of Portugal, with the known radiometric ages pointing to
132 two distinct pulses (94-88 Ma and 75-69 Ma) of magmatism (Miranda *et al.*, 2009). However,
133 some discrepancy with paleomagnetic data has been noticed suggesting that some of the
134 older geochronology results (namely those using K-Ar) should be reevaluated (Neres *et al.*,
135 2018). These occurrences include the sub-volcanic alkaline intrusions of Sintra, Sines and
136 Monchique, with multiple suites of granites, syenites, gabbros and nepheline syenites (78-71
137 Ma., K-Ar, Rb-Sr and U-Pb) (e.g. Alves, 1964; Wright, 1969; Sparks and Wadge, 1975; Rock,
138 1982; Miranda *et al.*, 2009; Grange *et al.*, 2010). In addition, effusive and explosive sequences
139 are described in the Lisbon Volcanic Complex (LVC) (~73 Ma, K-Ar) composed of basaltic
140 pyroclastic successions, lava flows and remnants of volcanic feeders (Alves *et al.*, 1980;
141 Ramalho *et al.*, 1993; Miranda *et al.*, 2009), along with multiple dykes and sills, from which the
142 Lomba dos Pianos, Paço de Ilhas (~88 Ma, K-Ar) or the Foz da Fonte (~94 Ma, Ar-Ar) are the
143 most expressive examples (Miranda *et al.*, 2009; Neres *et al.*, 2014) (Fig. 1). In southern
144 Portugal, several other manifestations can be observed, with multiple dykes, with ages up to

145 69 Ma (Grange *et al.*, 2010), crosscutting the Cretaceous sequence (see also Miranda *et al.*,
146 2009, and references therein). In addition to these observations, multiple magnetic anomalies
147 tentatively assigned to magmatic intrusions of this same cycle have been recently investigated
148 as part of the wider evidence of the extension of this province. Among these, the most
149 prominent corresponds to the Estremadura Spur Intrusion (ESI) and the Guadalquivir-
150 Portimão intrusion (Neres *et al.*, 2018; Escada *et al.*, 2019; Simões *et al.*, 2020), which bear
151 implications on the sourcing, processes and distribution of sub-lithospheric igneous material
152 in the central to north Atlantic region (Grange *et al.*, 2010; Merle *et al.*, 2019).

153 The Estremadura Spur, located on the central WIM and offshore the Lisbon region, is an
154 uplifted hinge zone, bounded by two perennial first-order strike-slip zones, the Tagus and the
155 Nazaré Fault Zones, both of which have played a major role in segmenting the WIM (Fig. 1)
156 (Alves *et al.*, 2009; Pereira *et al.*, 2017). Here, the Late Cretaceous strata are strongly
157 deformed as a result of NE-SW shortening of the margin during the Campanian-Early
158 Paleocene, which resulted in generalised folding and reverse faulting, ultimately crosscut by
159 a regional unconformity of Maastrichtian-Danian(?) age (Martín-Chivelet *et al.*, 2019; Pereira
160 *et al.*, 2021). Tectonic inversion resumed in the Tertiary with two main pulses of shortening,
161 by the mid-Eocene and Oligo-Miocene, recording the progressive rotation of the stress field
162 towards a NW-SE direction that ultimately shaped the current geometry of the drifting margin.
163 Deformation in the Estremadura Spur is also affected by the emplacement of a voluminous
164 laccolith exceeding 942 km³ (the ESI in Escada *et al.*, 2019; Pereira *et al.*, 2021). This is similar
165 to the Sintra intrusion, where folds and associated ring to radial dykes, and sills that can be
166 observed on outcrops (Alves, 1964; Ramalho *et al.*, 1993; Kullberg and Kullberg, 2017;
167 Terrinha *et al.*, 2017). The ESI becomes evident on geophysical potential field anomalies,
168 including free-air gravimetric anomaly exceeding 50 mGal and a total magnetic field (IGRF
169 removed) of 90 nT, and on high-resolution seismic datasets (Escada, 2019; Escada *et al.*,
170 2019).

171 Dredge samples collected at the exposed top of the Fontanelas volcano revealed a suite
172 of alkaline lava flows (mostly pillow lavas and hyaloclastites) ranging from foidite to alkaline
173 basalt and assigned to a sub-lithospheric mantle source (Miranda *et al.*, 2010). According to
174 the same authors, despite the lack of radiometric ages, but based on the geochemical
175 signatures, the Fontanelas volcano is considered to be part of the same Late Cretaceous
176 alkaline cycle observed onshore.

177 3. DATA AND METHODS

178 The analysis of the distinct magmatic features on the central WIM was accomplished by
179 interpreting different exclusive datasets of high-resolution seismic surveys, that include 2D
180 Two-Way Time (TWT) Post-Stack Time Migrated and 3D Pre-Stack Depth Migrated (PSDM)

181 seismic (Fig. 1). Seismic data was processed with zero phase and interpreted using normal
182 polarity according to the standards of the Society of Exploration Geophysicists, where an
183 increase in acoustic impedance corresponds to a positive red reflection and a decrease in
184 acoustic impedance is displayed in black.

185 The estimation of seismic resolution of sills and lava flows, in the absence of any direct
186 measurements or calibration, was achieved by considering a single velocity value of 5500 m/s,
187 an approximation similar to values published in literature (e.g. Bartetzko *et al.*, 2005; Magee
188 *et al.*, 2015). Considering the range of dominant frequencies at the interval of interest, of ~25
189 Hz, here estimated as a function of ~1/4 of the wavelength, the dataset allows to resolve
190 igneous features of around 55 m thick. Despite the limitations on seismic resolution in
191 resolving some of the thinner igneous features, that may be affected by tuning effects,
192 obtained values are considered suitable for an overall analysis of its dimensions and the
193 intruded rock volumes.

194 The recognition of sills on seismic data is usually accomplished by the visual identification
195 of strong reflectivity features that contrast with the surrounding sediments, which can display
196 a variety of forms and stratal relationships (e.g., planar, saucer-shaped, transgressive or
197 combinations of these) (e.g. Planke *et al.*, 2005; Schofield *et al.*, 2012; Jackson *et al.*, 2013;
198 Planke *et al.*, 2015). Moreover, as result of magma injection into pre-existing sedimentary
199 deposits, sills are often associated with forced folding of the overlying strata, allowing to
200 estimate the approximate age of magma emplacement at depth (Jackson *et al.*, 2013; Magee
201 *et al.*, 2017; Niyazi *et al.*, 2021a).

202 The vertical thickness of the individual sills was obtained directly from the PSDM seismic
203 volume in depth domain, by mapping the top and base reflections, and by measuring a single
204 value at the apparent thickest point. This value was later multiplied by its calculated area to
205 provide a notional volume of emplaced magma of the sills.

206 The volumes for individual lava flows were obtained with Petrel interpretation software, by
207 visually filtering the 3D volume and generating geoprobes that highlight the very-high
208 amplitudes from the PSDM seismic, in depth domain. Subsequently, the geoprobes were
209 converted to individual 3D geobodies, each providing the output of an approximate rock
210 volume that allow estimating a total volume of these lava flows.

211 In order to constrain the nature and any relations of extrusive features with neighbouring
212 volcanic edifices, as well its implications on the investigation of the magmatic cycle, lava flows
213 interpreted in this work are compared with examples observed in distinct geographical and
214 magmatic settings (Thomson, 2004; Planke *et al.*, 2017; Reynolds *et al.*, 2017b; Sun *et al.*,
215 2019; Bischoff *et al.*, 2020). Aiming to investigate the internal structure, build-up mechanisms
216 of the Fontanelas volcano and its implication for constraining the style of volcanism, a

217 comparison is established with previously documented buried volcanic edifices worldwide
218 (Magee *et al.*, 2013; Reynolds *et al.*, 2017a; Bischoff *et al.*, 2019; Sun *et al.*, 2019).

219 In the absence of any direct correlation with boreholes in the submerged area, seismic
220 stratigraphy criteria were used to characterize the distinct depositional mega-sequences
221 (*sensu* Hubbard *et al.*, 1985). In parallel, relative age constrain of the identified magmatic
222 features and associated sedimentary deposits was underpinned by regional geological
223 information of the main depositional strata in which coeval magmatism is described (Witt,
224 1977; GPEP, 1986; Azerêdo *et al.*, 2003; Rey *et al.*, 2006; Alves *et al.*, 2009; Miranda *et al.*,
225 2009; Pereira *et al.*, 2021).

226 **4. RESULTS**

227 In this section new evidence is presented for the occurrence on the offshore the central
228 WIM of distinct Late Cretaceous magmatic manifestations and their plumbing systems (Fig.
229 1). This includes the detailed analysis of numerous sills intruding this segment of the margin,
230 the description of a large volcanic edifice (the Fontanelas Volcano) with evidence of secondary
231 volcanic features, and its associated lava flows.

232 **4.1. SILLS**

233 One of the key testimonies of this magmatic event is the presence of multiple sills that were
234 previously reported in the region (Pereira and Barreto, 2018; Simões *et al.*, 2020; Pereira *et*
235 *al.*, 2021), although incompletely described and assessed for its significance; this is better
236 accomplished in this study, which entails the clarification of some of these aspects.

237 On the Estremadura Spur region numerous sills and sill complexes can be identified on 3D
238 seismic (Figs. 3, 4 and 5), and on outcrops (Fig. 6), from which 120 seismic features were
239 investigated in detail for this study, namely by performing the analysis of their geometry,
240 relative age and areal distribution. Characterised by high amplitudes on seismic data (Figs, 4,
241 5 and 7), predominantly intruding the unconformity-bounded sequence 5b (Turonian to mid-
242 Campanian age, Fig. 2), sills are mostly of layer parallel to slightly saucer-shaped type
243 showing on average 25-30 m thick intrusions (maximum of ~70 m) and an area of about 5
244 km², with the largest one reaching 59 km². These dimensions are comparable to what is
245 observed in one of the best exposed examples of sills on onshore outcrops, the basalts of the
246 Lomba dos Planos sill (30-40 m thick), observed on a shoreline cliff located north of the Sintra
247 massif (Figs. 1 and 6A-C). Despite the widespread distribution in the study offshore area, three
248 main clusters of sills can be identified, namely in the vicinity of the Fontanelas Volcano, the
249 ESI and in a central area in between the two (Figs. 3 and 4). The depth of sill emplacement
250 commonly corresponds to 250-500 m below the base of seismic sequence 5c. However, a

251 more detailed analysis on the depth and timing of emplacement is hindered by the strong
252 deformation and erosion of the stratigraphic boundaries.

253 In the area of the Fontanelas Volcano a group of at least 19 sills can be observed (Fig. 3).
254 Some form sill complexes, while others occur isolated around the perimeter of the volcanic
255 edifice, revealing a dominant layer parallel to slightly saucer shape geometry.

256 A cluster of over 15 sills of dominant layer parallel geometry can also be observed in the
257 central area of the survey (Fig. 5A). Here, an outstanding ~ 15 km² slightly saucer shape sill
258 (approximately 30 m thick, intruding unit 5b) exhibits evidence for forced folding and faulting
259 of overlying strata (Fig. 7A-B). Folding is marked by an unconformity overlain by onlaps of
260 depositional unit 5c, which ultimately provides constraints to the age of emplacement. South
261 of Lisbon, the onshore Foz da Fonte dolerite sill (98 ± 3.9 Ma; Miranda *et al.*, 2009) intrudes
262 Albian strata (Fig. 6F), an example described in detail by Kullberg and Kullberg (2017),
263 providing one of the few documented cases on outcrop to suggest evidence of forced folding.

264 Sills associated with the ESI stand out both atop the laccolith or around it, as highly
265 reflective amplitudes (Fig. 5A and 5C). Despite issues in seismic imaging mainly due to limited
266 acquisition and/or processing parameters, sills in this area are dominated by layer parallel and
267 slightly saucer shaped, although in this region a few clear planar transgressive sills can be
268 identified. In this area, a sill complex including an elongated 27 km² sill (maximum length of 9
269 km and 5 km wide, and about 40 m thick) (Fig. 7C-D), with slightly saucer shape geometry,
270 also showing a peculiar pedunculate to concave shape, is interpreted to represent the locus
271 of the feeder system associated to this cluster of intrusions, below which, some dimming of
272 seismic reflections and postulated faults occurs, possibly revealing the presence of magma
273 conduits. Analogue magmatic features can be observed on outcrop of the Sintra laccolith with
274 multiple crosscutting dikes and sills of trachytic-basaltic nature (Alves, 1964; Ramalho *et al.*,
275 1993) (Fig. 6D-E). Similar examples are also interpreted on seismic sequences of the Rockall
276 Trough, showing sill clusters associated with an intrusion (Archer *et al.*, 2005).

277 Notwithstanding some limitations in the interpretation of some magmatic features and the
278 incomplete coverage of the Estremadura Spur area, an estimation of the intruded rock volume
279 points to an approximate value in excess of 180 km³ for the total number of mapped sills.

280 **4.2. THE FONTANELAS VOLCANIC EDIFICE**

281 The Fontanelas volcano stands out on bathymetry surveys as a 500 m-tall physiographic
282 feature on the otherwise smooth recent sediment covered seafloor (Miranda *et al.*, 2010) (Fig.
283 3). Here, we present the details on both external and internal architecture of the volcanic
284 edifice (Figs. 3, 9 and 10), aiming to later clarify the nature of the extrusive event, and
285 ultimately to address the implications for the understanding of the magmatic cycle in West
286 Iberia and the Atlantic.

287

4.2.1. EXTERNAL ARCHITECTURE OF THE VOLCANO

288

289

290

291

292

293

294

295

The analysis of the external morphology of the Fontanelas volcano was performed by mapping the top and base of the edifice both on 2D TWT and 3D PSDM seismic datasets. Overall, the geometry of the volcanic edifice reveals the presence of two distinct summits, although without clear evidence for craters or calderas (Figs. 8, 9 and 10). This is interpreted as a structural feature of the magmatism responsible for the build-up of the volcano rather than post-eruptive erosion, given that well-developed diatremes would be visible in the seismic structure of the edifice, if they were present. The overall morphology of the Fontanelas volcanic edifice is, nevertheless, eroded to some extent.

296

297

298

299

300

301

302

303

304

305

306

307

308

309

310

311

312

313

314

The general geometry of the Fontanelas reveals that it extends over a basal area of 500 km², with its shape characterised by an ellipsoid NE-SW trend, with approximate dimensions on the longer axis of about 30 km (Length, L) and 25 km (Width, W) on the shorter segment (Fig. 8). Based on the 2D mapping of the top and bottom of the volcanic edifice, a base-case isochron TWT thickness map was calculated, by applying an approximate interval velocity for basaltic rocks of 5500 m/s. Accordingly, we estimated the total height (H) of the volcano, which is of up to 2800 m (Fig.8). Nonetheless, acknowledging uncertainty of our estimations, or possible variations on the overall properties of the volcanic edifice (see Magee *et al.*, 2015 for the discussion on rock properties, and references therein), the total height could vary from 2250 m (using a velocity of 4000 m/s) to 3350 m (using 6000 m/s). This base-case analysis allows estimating some notional aspect ratios such as ellipticity (L/W) of 1.2 and a Height vs Length ratio (H/L) of ~0.09, which can be broadly compared in terms of its morphology to present-day polygenetic composite volcanoes (e.g. Grosse *et al.*, 2012; Grosse *et al.*, 2013), despite some limitations that allow comparing recent and ancient volcanoes. Moreover, based on the interpreted top and base of the edifice, an approximate total rock volume of 327 km³ was calculated, which compares with other examples worldwide (Silva and Lindsay, 2015) and can fit to the category of shield to composite volcanoes, both in terms of the H/L ratio and rock volume. These aspects combined, can be used later to assess the nature of volcanism and its implications.

315

316

317

318

319

320

In order to investigate the conditions in which the volcano originated, namely for the sub-aerial or submarine paleo-topographic controls, we compared our data with buried volcanoes on the northern South China Sea (Sun *et al.*, 2020), in which typical hydromagmatic volcanic edifices extruded under shallow water conditions. In contrast to the features described by these authors, the Fontanelas Volcano does not exhibit evidence of a well-developed diatreme.

321 **4.2.2. INTERNAL ARCHITECTURE AND VOLCANIC PLUMBING SYSTEM**

322 Similar to descriptions of other buried volcanoes worldwide (e.g. Bischoff *et al.*, 2017;
323 Bischoff *et al.*, 2019; Walker *et al.*, 2020), the internal structure of the Fontanelas volcano
324 reveals multiple outward-dipping reflections, interpreted to express the progressive growth of
325 the edifice (Fig. 9). Underlying the volcano, the seismic signal is characterised by noisy to very
326 discontinuous reflectors and dimmed amplitudes, which is interpreted as resulting not only
327 from seismic signal attenuation from the volcanic edifice itself, but also as likely revealing a
328 sub-vertical plumbing system. Comparable to other buried volcanic edifices (Bischoff *et al.*,
329 2017; Niyazi *et al.*, 2021a), despite the limited resolution, a similar volcano architecture is
330 expected in which, several high amplitude reflectors can be observed. Reduction of seismic
331 resolution is likely the indirect evidence of an underlying complex feeder system, comprising
332 not only the observed sills, but also elusive conduits, stocks or previous magma reservoirs.

333 **4.3. LAVA FLOWS**

334 Associated with the Fontanelas volcano, two main groups of high seismic amplitude
335 features are identified and strongly contrasting with surrounding strata (Figs. 3, 8, 10 and 11;
336 Table 1). At first sight, they that can be compared either with magmatic extrusive examples
337 (Planke *et al.*, 2017; Reynolds *et al.*, 2017b; Sun *et al.*, 2019) or with sill morphologies
338 (Thomson and Hutton, 2004; Schofield *et al.*, 2012; Magee *et al.*, 2017).

339 The first group includes five high-confidence features that are observed within stratigraphic
340 unit 5b (lava flows LF1 to LF5), dominantly along a continuous seismic reflector in which, the
341 distinct reflective bodies are laterally overlapping (Fig. 10). Detailed interpretation and seismic
342 amplitude extraction of each of these features reveals that they form individual elongated and
343 adjoined fan-like geometries clearly showing lobes with crenulated margins (Fig. 11A-E).
344 Although some of these morphological features share similarities with large sills, they lack
345 some of the key criteria that are typical of these intrusive entities, like cross-cutting strata or
346 their generally lower aspect ratio (length/width) translated in more sub-circular to elliptic shape
347 (e.g. Schofield *et al.*, 2012). Contrastingly, these seismic features are closely comparable to
348 lava flows described in the Atlantic North Sea or the South China Sea (Planke *et al.*, 2017;
349 Sun *et al.*, 2019). Accordingly, the interpreted features often reveal multiple elongated
350 geometries indicative of several events of nearly synchronous flow, forming fans along a
351 similar path of extrusion, likely controlled by pre-existing topography (see lava flows LF1, LF2
352 and LF3, Figs. 11A, B and E). Lava flow 3 (Fig. 10C), however, is characterised by a sheet-
353 like geometry with some lobate marginal crenulation and shows an irregular path, changing
354 from a westward direction of flow, towards a NW trend. Despite its distinct geometry, the
355 trajectory apparently shares a common vent with lava flows 1 to 4 (Fig. 11 and 12). This group
356 of pre-Fontanelas extrusive features points to a postulated location for extrusion that seems

357 related with a group of faults, likely inherited from the syn-rift extensional phase, later reworked
358 during inversion, as expressed by noteworthy tilting and folding of the late Cretaceous strata,
359 sills and the lava flows (Fig. 12). This common rooting, as well as their exact same
360 stratigraphic position, thus strongly suggest these lava flows were extruded during the same
361 eruptive event.

362 Lava flow 5, characterised by two individual and sub-parallel fan shape geometries, is
363 overall smaller in area and volume (Figs. 8 and 11E). LF5 is observed to overlay LF2,
364 suggesting that it is relatively younger than the former extrusive sequence (Fig. 10). Despite,
365 showing a distinct SW direction of flow when compared with the other lava flows (LF1-4),
366 suggesting that an alternative source of extrusion may have been present, LF 5 is considered
367 as part of the same extrusive event.

368 Aiming to obtain an approximation of the expelled volume of rock for pre-Fontanelas
369 extrusive event (Lava flows LF1 to LF5, Table 1), extraction of geoprobes (a 3D rendering tool
370 based on the extraction of high seismic amplitudes) for each lava flow was performed. This
371 approach indicates that altogether these features comprise a total of 2.7 km³ of magma that
372 was extruded during this event and for this location. This is an approximate value given this
373 analysis does not account for all possible lava flows imaged by seismic data, the time-depth
374 conversion uncertainties associated with the final PSDM seismic volume,

375 A second group of seismic high-amplitude features is directly associated with the base and
376 top boundary of the volcano (lava flows LF6 to LF8), which is stratigraphically distinct (and
377 younger) than the lava flows described above. These features have a clear dissimilar shape
378 relatively to those previously described, with its seismic features revealing dendritic and sheet-
379 like geometries (Fig. 11F-H). These are characterised by high amplitudes with very elongated
380 channelised features, typically forming dendritic lobes at its terminations and interpreted here
381 as lava flows, in which the source can be tracked to the volcanic edifice itself. Lava flows LF6
382 and LF7 are interpreted at the base of the volcanic edifice, whereas lava flow LF 8, located in
383 the flank is associated to one of the latest extrusive events. The relative stratigraphic position
384 and geometry of these lava flows contrasts with those described previously, which bears
385 implications on the type of volcanism under analysis in each case (see discussion below).

386 **5. DISCUSSION**

387 West Iberia records multiple events of intra-plate magmatism, in which, the so called Late
388 Cretaceous alkaline cycle is often considered as part of a larger magmatic province that
389 extends throughout the peri-Atlantic domain (e.g. Matton and Jébrak, 2009; Miranda *et al.*,
390 2009; Grange *et al.*, 2010; Merle *et al.*, 2019). Adding to this understanding, new evidence
391 from the subsurface, including its tectono-magmatic insights, helped to bring forward an
392 updated view on the larger extent, significance and implications on this cycle (Pereira *et al.*,

393 2017; Neres *et al.*, 2018; Pereira *et al.*, 2021). Building on our new observations, that include
394 the details on the presence a large volcanic edifice (the Fontanelas Volcano), along with lava
395 flows and also, numerous sills and sill complexes, as part of a complex magmatic plumbing
396 system, a discussion is herein presented, aiming to elaborate on the type, timing and
397 magnitude of magmatism, as well as the implications for the wider WIM magmatic province,
398 as a whole.

399 **5.1. ASSESSING THE TYPE OF MAGMATISM**

400 In the absence of any direct methods to investigate the buried Late Cretaceous magmatic
401 activity on the Central WIM, the type of magmatism is here discussed based on seismic
402 geomorphology observations. It is also compared to evidence of ancient plumbing systems
403 (either cropping out on the onshore WIM or to other regions imaged by seismic reflection
404 methods), as well with examples from extant volcanic regions worldwide.

405 The analysis of the sills and sill complexes intruding this segment of the margin shows that
406 these are mainly distributed in three domains, namely, 1) in the vicinities of the ESI; 2) the
407 Fontanelas volcano; and 3) at a central area in between these two entities. Based on the fault
408 pattern and the location of the intrusions (Fig 4), the clustering of sills is interpreted to have
409 been controlled by pre-existing structural weaknesses inherited from the previous sin-rift
410 tectono-sedimentary evolution, which would favour distinct areas for magma ascent and
411 emplacement. The role of structural inheritance controlling the magma emplacement in the
412 Lusitanian Basin, is also reported to Jurassic-Cretaceous transition dykes and sills, associated
413 with multiple salt diapirs (Mata *et al.*, 2015; Davison and Barreto, 2021).

414 In the Estremadura Spur area, Late Cretaceous sills tend to be emplaced in areas where
415 WNW-ESE reverse faulting is noticeable (Fig. 4). Here a group of reverse faults (Figs. 5B and
416 7A-B) are observed underlying the sills. Evidence of this tectonic imprint acting as conduits is
417 also suggested by inclined seismic reflections underlying the ESI (feeder dykes?), as well as
418 dimming of seismic data along with upward bending reflections underlying the Fontanelas
419 volcano, as part of the wider plumbing system (Figs. 3, 5 and 9). Similar evidence on the
420 detailed imaging of plumbing systems is discussed with examples from the southeast
421 Australian Margin and the Faroe-Shetland region (McLean *et al.*, 2017; Niyazi *et al.*, 2021a;
422 Niyazi *et al.*, 2021b). Accounting for the position of the sills in relation with the volcanic edifice
423 and any controls from structural inheritance (McLean *et al.*, 2017; Barrier *et al.*, 2021; Niyazi
424 *et al.*, 2021b), these igneous features are interpreted to be associated with underlying syn-rift
425 faults; these faults probably acted as conduits for magma ascension to its final position within
426 a pre-volcanic sequence (dominantly unit 5b) and in some cases, extruding to surface and
427 contributing to the build-up of the volcanic edifice (Fig. 4). Another relevant aspect of sills in
428 the vicinity of the ESI is the similarity to what is observed around the Sintra massif (Fig. 6D-

429 E) (Alves, 1964; Sparks and Wadge, 1975; Ramalho *et al.*, 1993). Sills are distributed both on
430 top of the ESI laccolith and around it, what can be interpreted as being part of a similar complex
431 network of ring and radial dykes.

432 The type of magmatism can be diagnosed in more detail by the analysis of its lava flows.
433 Our observations allowed the discrimination of two groups of lava flows, with distinct location,
434 geometries, and relative time of emplacement. A first group of lava flows (LF1–LF5, Fig. 11),
435 pre-dating the build-up of the Fontanelas volcano, and observed south of the volcanic edifice,
436 include fan- and lobate-shaped lava flows with crenulated lobate margins, extending on a
437 kilometre scale towards the NW, support a distinct source from the main volcanic feeding
438 system. These morphologies are very distinctive and are clearly akin to voluminous “inflated”
439 sheet or 'a'ā lava flows extruded under high to very high effusion rates, such as those
440 described in historical subaerial eruptions (e.g., at Hawaii Peterson and Tilling, 1980), at Fogo
441 volcano, (Mata *et al.*, 2017), in Iceland (Planke *et al.*, 2017), or such as those described at
442 deep-sea submarine eruptions on seamounts and mid-ocean ridges (e.g. Axial Seamount and
443 East Pacific Rise; Chadwick Jr. *et al.*, 2013; White *et al.*, 2015). The root of these lava flows
444 converges to the south of the volcanic edifice, suggesting that the vent that fed them may be
445 located in this area, although not fully evident on seismic data. Moreover, the lack of a
446 significant volcanic edifice at this exact stratigraphic level, as well as the convergence of the
447 root of these flows along an elongated area, suggests that these lava flows resulted from a
448 voluminous fissure-fed effusive eruption, alike those produced along the rift zones of Iceland
449 (such as the 2018 Holuhraun eruption), in Afar (Ethiopia), or at the Axial Seamount, in the
450 present day.

451 Assuming that this first group of lava flows (LF1-5) were extruded during a specific and
452 relatively time-constrained eruption (as their common origin, geometry and stratigraphic
453 position suggest) their combined volume amounts to $2.69 \times 10^9 \text{ m}^3$, which is significant. If we
454 consider a density ranging in 2600 to 2800 kg/m^3 for the basalts that compose these flows¹,
455 this combined volume corresponds to a total extruded mass of $7.0\text{--}7.5 \times 10^{12} \text{ kg}$, leading to
456 an estimated eruption magnitude of 5.8–5.9 (as defined by Pyle, 2015). For comparison, these
457 values are in the same range of some of the largest effusive eruptions (e.g., the June 1950
458 Mauna Loa eruption) registered in historical times, thus attesting to the very large size of the
459 eruptive episode and its relative importance within the context of what is generally considered
460 a magma-starved margin.

461 Considering this evidence, and since these fissural lava flows pre-date the build-up of the
462 Fontanelas volcano, we interpret that these features constitute one of the first expressions of

¹ The bulk of the volume of thick or “inflated” submarine sheet or subaerial 'a'ā lava flows corresponds to the coherent, generally vesicle-poor interior/core, and therefore the density of such flows typically approximates the values for non-vesicular basalt.

463 magmatic extrusion in the area. Effectively, these lava flows attest to an earlier, dominantly
464 effusive, and highly voluminous fissure-fed eruptive phase of the Late Cretaceous magmatism
465 in this sector of the margin, here documented for the first time and a unique description for
466 ancient volcanic systems.

467 The second group of lavas, either at the base (depicting the first flows) or at the top flank
468 of the Fontanelas volcano, is directly associated with prolonged volcanic activity at this
469 eruptive vent. In contrast with the extrusive features described above, these lava flows are
470 characterised by an overall channelised/dendritic geometry forming lava lobes and digitations
471 at its terminations, characteristics that are typical of lava flows extruded under low effusion
472 rates. This morphology suggests an emplacement similar to that of present-day lobate
473 pāhoehoe flows or to submarine lobate flows (see Kereszturi *et al.*, 2015 and references
474 therein).

475 The morphology of the Fontanelas volcanic indicate the presence of two distinct
476 culminations, which along with its complex internal structuration (although not fully resolved
477 on 3D seismic data), suggests that this an example of a compound volcano, with two main
478 eruptive centres. This interpretation is reinforced by the presence of multiple vertical zones of
479 dimmed seismic reflectivity under each inferred volcanic centre, interpreted as volcanic feeder
480 conduits. Additionally, the evidence of distinct internal outward-dipping reflections in the
481 Fontanelas edifice, with these internal reflections not being parallel to the top surface of the
482 volcano, indicates that through time the edifice has grown to different shapes and by building
483 distinct layers, to ultimately reach its final architecture and size as a polygenetic volcano.

484 A fundamental question that is worth asking concerns the subaerial vs. submarine nature
485 of the described volcanic features/edifices. The answer to this question is not straightforward
486 and the different possibilities are worth discussing here. The morphology of the described lava
487 flows is both compatible with subaerial or deeper water features, but is not compatible with
488 shallow water volcanism. At shallow water environments (i.e. <150 m water depth), hydrostatic
489 pressures are low enough to allow for the production of large quantities of steam when the hot
490 magma contacts the water, resulting in either surtseyan or taalian eruptions (depending of the
491 water/magma ratio), both of which are violently explosive and lead to the generation of large
492 tuff cones and rings and well-developed diatremes (see Sheridan and Wohletz, 1981;
493 Verwoerd and Chevallier, 1987; Sohn, 1996; Sun *et al.*, 2019). These, however, are not
494 features observed at the Estremadura Spur. Conversely, both the Fontanelas volcano and the
495 lava flows sequence that precedes this edifice are dominantly effusive and lack large craters
496 and diatremes. It is therefore highly unlikely that these features were extruded under shallow
497 water conditions.

498 A subaerial origin for these features is possible – and to some extent appealing, given that
499 higher similarity of the described lava flows with other lava flows extruded on land, but poses

500 some challenges. Indeed, albeit being eroded at the crest, the overall morphology and internal
501 structure of each of the individual volcanic edifices is compatible with largely subaerially-built
502 polygenetic composite volcanoes. If so, the Fontanelas volcano and adjacent secondary vents
503 would have been built by bimodal volcanism (explosive and effusive) in an essentially
504 subaerial environment, with eventually some subaerially-extruded flows entering a shallow
505 water environment at the foot of the volcano (if the lobate flows described above correspond
506 to submarine flows and not pāhoehoe flows). This could be compared with evidence from
507 outcropping features in the coeval LVC where the main subaerial volcanic deposits, including
508 pyroclastic deposits interlayered with lava flows, are observed blanketing an unconformity
509 cross-cutting upper Cenomanian limestones with rudists and carbonate conglomerates (Aires-
510 Barros, 1979; Alves *et al.*, 1980; Marques *et al.*, 1998; Manupella *et al.*, 2011). In the Lisbon
511 region, post-Cenomanian strata are absent, with the only preserved deposits described in the
512 northern Lusitanian Basin and in the offshore (e.g. Witt, 1977; Rey *et al.*, 2006) (Fig. 2). Strata
513 include fluvial-deltaic siliciclastic and shallow marine/transitional carbonates of Turonian to
514 Maastrichtian age, suggesting that after a period of widespread margin exposure, shallow
515 marine deposition resumed and progressively flooded the Estremadura Spur (sequence 5C),
516 blanketing the exposed (?) volcanic edifice. The fact, however, that the described volcanic
517 sequences are within a stratigraphic unit composed of limestones (Fig. 2), poses thus a
518 paleoenvironment problem, requiring multiple sea-level oscillations to intercalate supposedly
519 subaerial volcanic products with marine limestones.

520 The most likely scenario is thus, for the described volcanic sequences, to have been
521 extruded in a submarine environment, at intermediate water depths, necessarily
522 comprehended above the carbonate compensation depth and below the critical depth for the
523 onset of hydromagmatic explosive volcanism (~150 m). This scenario is also supported by the
524 fact that mafic pillow lavas and hyaloclastites were dredged from the top of the Fontanelas
525 volcano (Miranda, 2010). In addition, the existence of possible erosional terraces at the flanks
526 of the Fontanelas volcano (see Fig. 9), suggests that, despite the Tertiary strata blanketing
527 the volcanic edifice, the edifice was possibly eroded posteriorly by marine erosion during sea-
528 level oscillations. The edifice nevertheless constituted a significant landmark from the late
529 Cretaceous to the Paleogene, when ultimately, a combination of relative sea-level rise, marine
530 deposition and tectonism of the margin fully submerged and buried the Estremadura Spur
531 under the transgressive sequence we see today.

532 **5.2. TIMING OF MAGMATIC EVENTS**

533 In the absence of age dating for the igneous rocks in this offshore area, the timing of
534 magmatic events must be tentatively established based on the seismic-stratigraphic
535 framework, underpinned by the regional setting. As a whole, and as shown in this study, the

536 timing of these magmatic activity is bounded between units 5a and 5c ranging from Turonian
537 to Campanian (~94 to 72 Ma). This indicates that the reported magmatic activity should be
538 considered as part of the third Mesozoic cycle of magmatic activity at the WIM, as already
539 suggested by Miranda *et al.* (2009) for the Fontanelas volcano, based on its alkaline
540 characteristics.

541 The analysis of the relative stratigraphic position of the distinct manifestations of
542 magmatism in the Estremadura Spur suggest that two pulses of magmatic activity have
543 occurred. Accordingly, the age constraint of the main magmatic events take into account: 1)
544 the onlap-bounded unconformity of base unit 5c (of interpreted mid Campanian age),
545 associated with the onset of the ESI intrusion and forced folding (Figs. 5 and 7); and 2) the
546 Base Tertiary Unconformity (Maastrichtian-Danian?) (Fig. 2).

547 The first magmatic pulse is marked by the effusive event within sequence 5b, preceding
548 the intra-Campanian unconformity, with the extrusion of voluminous lava flows (LF1 to LF5)
549 (Figs. 10 and 11) fed by fissural volcanism. This means that the first magmatic event is
550 consequently older than the onset of intrusion/extrusion of the ESI and the Fontanelas
551 volcano. Considering these criteria, a tentative Coniacian to lower Campanian age (~ 90 to 84
552 Ma) for this initial event is considered, a period that can be compared with the first magmatic
553 pulse also observed at outcrops (e.g., Lomba dos Pianos), but likely younger than the Foz da
554 Fonte sill (93.8±3.9 Ma; Miranda *et al.*, 2009), the first documented and undoubtful example
555 of the magmatic cycle onshore (Figs, 1, 2 and 6).

556 The second and more voluminous magmatic pulse can be positioned during the mid to late
557 Campanian (~80 to 72 Ma), as it apparently slightly precedes the onlap of unconformity
558 bounded unit 5c, with evidence of forced folding (Fig. 7), and includes the ESI laccolith, the
559 Fontanelas volcanic edifice and most of the sills and sill complexes. Combined, these two
560 interpreted pulses of magma in the Estremadura Spur are coeval with those (94-88 Ma; 75-
561 72 Ma) observed onshore (Miranda *et al.*, 2009), thus providing significant assurance to our
562 analysis.

563 **5.3. MAGNITUDE OF MAGMATISM**

564 To investigate the approximate magnitude of the combined magmatic event, partial rock
565 volumes have been estimated, including the ESI laccolith, the high confidence sills, the
566 Fontanelas volcano and its associated lava flows. Despite some limitations on the dataset and
567 the methods allowing to quantify the different rock volumes, the estimated volumes of
568 magmatic material are not an absolute value but provide an indication of the overall magnitude
569 of the wider event. For the ESI laccolith intrusion, Pereira *et al.* (2021) report a total volume of
570 942 km³. From the data obtained for this study, we estimate that the sills account for ~180 km³
571 of intruded material, the Fontanelas volcano (including lava flows at base and top), has yielded

572 a base-case around 327 km³ of rock (ranging from 250 to 380 Km³). For the associated pre-
573 Fontanelas lava flows, the lower estimate points to an excess of 2.7 km³ of extruded magma.
574 Altogether, considering the individual or groups of magmatic features, a total volume of
575 magma of 1452 km³ is estimated to have been extruded/intruded at the Estremadura Spur,
576 on a total area of about 2500 km². These values, which are an absolute minimum estimate
577 (not excluding additional unresolved magmatic features in the area or others that may be
578 located outside the high-resolution 3D dataset, and not accounted herein), confirm that the
579 post-rift magmatism that took place at the WIM during the Late Cretaceous was indeed very
580 sizeable. This is more so, when the overall volume of pene-contemporaneous magmatism
581 found onshore is also considered.

582 This places the Late Cretaceous magmatism as a dominant event in the region, spreading
583 out over an area of 30.000 km² on the whole proximal WIM. This portion of the wider magmatic
584 province reveals clear implications in what concerns the thermal evolution of the margin and
585 its geodynamic context. Although limited by scarce data, evidence from petroleum systems
586 modelling and oil typing on the Porto and Lusitanian Basins (Beicip-Franlab, 1996; Ferreira,
587 2017) suggest that during this period the impact of a widespread and deep heat source may
588 have thermally controlled conditions for fluid flow in the continental crust.

589 The third cycle post-dated the lithosphere breakup by some 30 Ma (Miranda *et al.*, 2009
590 and references therein) and presents geochemical characteristics compatible with a dominant
591 asthenospheric signature (Miranda *et al.*, 2009; Grange *et al.*, 2010). Acknowledging the wider
592 expression and magnitude of Late Cretaceous alkaline intra-magmatism may condition the
593 view on the dominant processes controlling this event, whether related to mantle plume-
594 derived melting leading to the formation of “hotspots” on the margin (Oyarzun *et al.*, 1997;
595 Grange *et al.*, 2010; Merle *et al.*, 2019) or, alternatively, as the combined product of edge-
596 driven convection and continental insulation, that would have favoured magma ascent from a
597 shallow mantle source (e.g. Matton and Jébrak, 2009). Recent seismic tomographic data
598 (Civiero *et al.*, 2021) favours the plume model with several partially coeval mantle upwellings
599 (plumes, s.l.) explaining the abundance of Late-Cretaceous to Cenozoic intraplate magmatism
600 in a vast region of the Central East Atlantic. According to this study such plumes are anchored
601 at the Central East Atlantic Anomaly, ponded below the 660 km anomaly.

602 **6. CONCLUSIONS**

603 The Late Cretaceous alkaline cycle on the central West Iberian Margin is revealed to
604 include the Fontanelas volcano with its associated lava flows and the multiple manifestations
605 of a shallow magmatic plumbing system, including numerous sills, and the Estremadura Spur
606 Intrusion.

607 Sills are characterised by multiple geometries that range from planar to saucer-shaped,
608 (occasionally forming sill complexes), dominantly intruding 250-500 m below the top of unit 5B
609 of mid-Campanian age. On average they are 30-40 m thick, with individual areas that can
610 reach 59 km². These intrusive features are clustered in three main areas, an observation that
611 suggests that its emplacement was largely controlled by inherited syn-rift faulting.

612 The analysis of both external and internal architecture of the Fontanelas volcano reveals
613 that the volcanic edifice denotes a complex geometrical and extrusive evolution, marked by
614 successive periods of growth, to ultimately form a two-summit stratovolcano reaching a total
615 height of ~2800 m. Two distinct groups of lava flows are identified around the volcano, that
616 include: 1) A cluster of five features of kilometre scale fan-shape to tabular crenulated
617 submarine sheet or 'a'ā lava flows, that precede the build-up of the Fontanelas edifice, created
618 by a large fissure-fed effusive eruption with an estimated magnitude of 5.8–5.9, comparable
619 to the June 1950 Mauna Loa eruption.; and 2) Dendritic and lobate lava flows (either
620 pahoehoe or submarine lobate flows) directly associated with the volcanic build-up.
621 Accordingly, the Fontanelas volcano is interpreted to represent an example of a composite
622 and compound volcanic edifice, possibly extruded at intermediate water depths
623 comprehended above the carbonate compensation depth and below the critical depth for the
624 onset of submarine explosive volcanism.

625 Magmatism on the central WIM is interpreted to have occurred during two main pulses: I)
626 Coniacian-lower Campanian(?) age, marked by the extrusion of the first lavas under fissural
627 volcanism; and II) the intrusion of the ESI, the Fontanelas volcano and most of the sills during
628 mid-late Campanian.

629 With a total volume of magma involved in this system (from the ESI, Fontanelas, lava flows
630 and sills) in excess of 1452 km³, the Late Cretaceous magmatic event is shown to represent
631 a sizeable event, both in extent and magnitude. This bears implications for the further
632 understanding of the peri-Atlantic alkaline province and for controlling any fluid flow to charge
633 prospective petroleum systems or by reducing crustal strength during tectono-magmatic
634 events.

635

636 **Acknowledgments**

637 The authors wish to thank the support of Partex Oil and Gas, for allowing the wider research
638 project to be implemented and for the permission to publish the data. R.R. acknowledges his
639 IF/01641/2015 “Investigador FCT” contract, funded by Fundação para a Ciência e Tecnologia
640 I.P (FCT). This work was supported by the project FCT/UIDB/50019/2020 - IDL funded by
641 FCT.

642

643 **Conflict of Interests**

644 The authors declare that there is no conflict of interests.

645

646 **Figures**

647 Figure 1. Location of the area of interest showing the distribution of magmatism on the
648 central West Iberian Margin. ESI – Estremadura Spur Intrusion, LVC – Lisbon Volcanic
649 Complex, AF – Aveiro Fault, NFZ – Nazaré Fault Zone, TFZ – Tagus Fault Zone, PSF –
650 Pereira de Sousa Fault, MPF – Marquês de Pombal Fault, MPFZ – Messejana-Plasencia Fault
651 Zone.

652 Figure 2. Stratigraphic framework of the West Iberian Margin showing the distinct
653 megasequences, lithostratigraphic units and evidence of the Late Cretaceous alkaline
654 magmatism. LBS – Lithosphere Breakup Sequence (Unit 5a).

655 Figure 3. Seismic line (in depth) across the Estremadura Spur, showing the evidence of
656 the Fontanelas volcano, the Estremadura Spur Intrusion with associated sills (red) and lava
657 flows (purple), as part of the larger magmatic plumbing system of the Late Cretaceous. BTU
658 – Base Tertiary Unconformity.

659 Figure 4. Map showing the location of the Fontanelas volcano, the dominant distribution of
660 sills (red) and lava flows (purple), and the Estremadura Spur Intrusion (ESI).

661 Figure 5. Seismic lines (in depth) showing the distribution and different geometry of sills (in
662 red) throughout the Estremadura Spur. Note that sills and sill complexes are dominantly
663 emplaced within sequence 5b. Location of seismic lines in figure 4.

664 Figure 6. Outcropping examples of the Late Cretaceous magmatism. A) Lomba dos Pianos
665 sill, as seen on Google Maps perspective, showing the relation between the Albian-
666 Cenomanian limestones and marls. Approximate thickness of the sill is 30-40 m. Lat:
667 38°53'36.22"N, Long: 9°26'18.00"W. B) Detail of the Lomba dos Pianos sill showing the top
668 contact with limestones, evidencing prismatic joints. View to the South. C) Detail of the basaltic
669 sill, showing zeolites filling fractures. D) Crosscutting trachytic-basaltic(?) ring dykes
670 associated with the Sintra intrusion, at Ponta da Abelheira. View to the South. Lat:
671 38°44'52.81"N; Long: 9°28'18.36"W. E) Trachytic-basaltic(?) dykes and sills crosscutting late
672 Jurassic limestones at Ponta da Abelheira, showing the landscape of the Sintra massif at a
673 distance. F) The Foz da Fonte sill intruding Albian limestones, an example of forced folding
674 associated with shallow magma emplacement; Lat: 38°27'3.91"N, Long: 9°12'6.25"W.

675 Figure 7. Details of sills intruding the Estremadura Spur. A) Seismic section showing an
676 example of a planar-slightly saucer chape sill intruding unit 5b, with forced folding and faulting
677 of overburden strata, with onlaps at base of sequence 5c. Note faulting at the edge of sill,
678 tentatively interpreted as conduit for magma emplacement. B) 3D view of the sill showing the
679 flanks of the sill. C) Sill complex intruding unit 5b, highlighting the presence of a saucer-shape

680 sill and possible magma conduit. D) 3D view of the sill, showing its complex geometry and
681 possible source of magma flow.

682 Figure 8. A) Thickness map of the Fontanelas volcanic edifice, based on 2D/3D seismic
683 data, with associated lavas (1 to 8), with interpreted flow directions from a common source.
684 Note the presence of secondary volcanic vents. B) TWT structural map of the Fontanelas
685 volcano.

686 Figure 9. TWT seismic lines across the Fontanelas volcano, highlighting the internal
687 structuration and build-up of the volcanic edifice (outward dipping reflectors), lava flows (in
688 purple), associated secondary vents and deep plumbing systems with multiple sills (in red).
689 Possible erosional terraces at the flank of the volcano suggest possible influence of
690 submergence and shallow water conditions.

691 Figure 10. Random seismic line across the southern flank of the volcano, showing pre-
692 Fontanelas lava flows (1 to 5) and syn-Fontanelas lava flows (6-8). See figure 8 for location,
693 figure 11 and Table 1 for details of the lava flows.

694 Figure 11. Plan view of seismic amplitudes of interpreted flows, showing multiple lava fans,
695 lobate to crenulated terminations. Arrows indicate likely direction of flow, in relation to its
696 interpreted source and the position of the Fontanelas volcano.

697 Figure 12. 3D perspective (in depth) of pre-Fontanelas lava flows and interpreted source
698 for fissural magmatism preceding the build-up of the main volcanic edifice. Note the
699 confluence of the origin of lava flows onto inversion faults, likely inherited from the syn-rift
700 architecture.

701

702 Table 1. Description and characteristics of the lava flows associated with the Fontanelas
703 volcano.

704

705 **Conflict of Interests**

706 The authors declare that there is no conflict of interests during this work nor for its publication.

707

708 **References**

- 709 Aires-Barros, L. (1979) Actividade Ígnea Pós-Paleozóica No Continente Português
710 (Elementos Para Uma Síntese Crítica). *Ciências da Terra*, **5**, 175-214.
711 Alves, C.a.M. (1964) Estudo Petrológico Do Maçico Eruptivo De Sintra. *Revista da Faculdade*
712 *de Ciências de Lisboa*, **XXII**, 124-289.
713 Alves, C.a.M., Rodrigues, A., Serralheiro, A. & Fria, F. (1980) O Complexo Basáltico De
714 Lisboa. *Comunicações dos Serviços Geológicos de Portugal*, **66**, 111-134.
715 Alves, T.M., Moita, C., Cunha, T., Ullnaess, M., Myklebust, R., Monteiro, J.H. & Manupella, G.
716 (2009) Diachronous Evolution of Late Jurassic-Cretaceous Continental Rifting in the
717 Northeast Atlantic (West Iberian Margin). *Tectonics*, **28**, TC4003.
718 10.1029/2008TC002337.

- 719 Archer, S.G., Bergman, S.C., Iliffe, J., Murphy, C.M. & Thornton, M. (2005) Palaeogene
720 Igneous Rocks Reveal New Insights into the Geodynamic Evolution and Petroleum
721 Potential of the Rockall Trough, Ne Atlantic Margin. *Basin Research*, **17**, 171-201.
722 <https://doi.org/10.1111/j.1365-2117.2005.00260.x>.
- 723 Azerêdo, A.C., Duarte, L.V., Henriques, M.H. & Manupella, G. (2003) *Da Dinâmica*
724 *Continental No Triásico Aos Mares Do Jurássico Inferior E Médio*. Instituto Geológico e
725 Mineiro, Lisboa, Portugal. 43
- 726 Barrier, A., Bischoff, A., Nicol, A., Browne, G.H. & Bassett, K.N. (2021) Relationships between
727 Volcanism and Plate Tectonics: A Case-Study from the Canterbury Basin, New Zealand.
728 *Marine Geology*, **433**, 106397. <https://doi.org/10.1016/j.margeo.2020.106397>.
- 729 Bartetzko, A., Delius, H. & Pechinig, R. (2005) Effect of Compositional and Structural
730 Variations on Log Responses of Igneous and Metamorphic Rocks. I: Mafic Rocks.
731 *Geological Society, London, Special Publications*, **240**, 255-278.
732 [10.1144/gsl.Sp.2005.240.01.19](https://doi.org/10.1144/gsl.Sp.2005.240.01.19).
- 733 Beicip-Franlab (1996) Geochemical Evaluation of the Lusitanian and Porto Basins, BEICIP-
734 FRANLAB, 18.
- 735 Bernard-Griffiths, J., Gruau, G., Cornen, G., Azambre, B. & Mace, J. (1997) Continental
736 Lithospheric Contribution to Alkaline Magmatism: Isotopic (Nd, Sr, Pb) and Geochemical
737 (Ree) Evidence from Serra De Monchique and Mount Ormonde Complexes. *Journal of*
738 *Petrology*, **38**, 115-132. [10.1093/petroj/38.1.115](https://doi.org/10.1093/petroj/38.1.115).
- 739 Bischoff, A., Nicol, A., Cole, J. & Gravley, D. (2019) Stratigraphy of Architectural Elements of
740 a Buried Monogenetic Volcanic System. *Open Geosciences*, **11**, 581.
741 <https://doi.org/10.1515/geo-2019-0048>.
- 742 Bischoff, A., Barrier, A., Beggs, M., Nicol, A., Cole, J. & Sahoo, T. (2020) Volcanoes Buried in
743 Te Riu-a-Maui/Zelandia Sedimentary Basins. *New Zealand Journal of Geology and*
744 *Geophysics*, **63**, 378-401. [10.1080/00288306.2020.1773510](https://doi.org/10.1080/00288306.2020.1773510).
- 745 Bischoff, A.P., Nicol, A. & Beggs, M. (2017) Stratigraphy of Architectural Elements in a Buried
746 Volcanic System and Implications for Hydrocarbon Exploration. *Interpretation*, **5**, SK141-
747 SK159. [10.1190/int-2016-0201.1](https://doi.org/10.1190/int-2016-0201.1).
- 748 Bronner, A., Sauter, D., Manatschal, G., Péron-Pinvidic, G. & Munsch, M. (2011) Magmatic
749 Breakup as an Explanation for Magnetic Anomalies at Magma-Poor Rifted Margins. *Nature*
750 *Geoscience*, **4**, 549–553. [10.1038/NGEO1201](https://doi.org/10.1038/NGEO1201).
- 751 Callegaro, S., Rapaille, C., Marzoli, A., Bertrand, H., Chiaradia, M., Reisberg, L., Bellieni, G.,
752 Martins, L., Madeira, J., Mata, J., Youbi, N., De Min, A., Azevedo, M.R. & Bensalah, M.K.
753 (2014) Enriched Mantle Source for the Central Atlantic Magmatic Province: New
754 Supporting Evidence from Southwestern Europe. *Lithos*, **188**, 15-32.
755 [http://dx.doi.org/10.1016/j.lithos.2013.10.021](https://doi.org/10.1016/j.lithos.2013.10.021).
- 756 Chadwick Jr., W.W., Clague, D.A., Embley, R.W., Perfit, M.R., Butterfield, D.A., Caress, D.W.,
757 Paduan, J.B., Martin, J.F., Sasnett, P., Merle, S.G. & Bobbitt, A.M. (2013) The 1998
758 Eruption of Axial Seamount: New Insights on Submarine Lava Flow Emplacement from
759 High-Resolution Mapping. *Geochemistry, Geophysics, Geosystems*, **14**, 3939-3968.
760 <https://doi.org/10.1002/ggge.20202>.
- 761 Civiero, C., Custódio, S., Neres, M., Schlaphorst, D., Mata, J. & Silveira, G. (2021) The Role
762 of the Seismically Slow Central-East Atlantic Anomaly in the Genesis of the Canary and
763 Madeira Volcanic Provinces. *Geophysical Research Letters*, **48**, e2021GL092874.
764 [10.1029/2021gl092874](https://doi.org/10.1029/2021gl092874).
- 765 Davison, I. & Barreto, P. (2021) Deformation and Sedimentation Processes, and Hydrocarbon
766 Accumulations on Upturned Salt Diapir Flanks in the Lusitanian Basin, Portugal. *Petroleum*
767 *Geoscience*, **27**, petgeo2019-2138. [10.1144/petgeo2019-138](https://doi.org/10.1144/petgeo2019-138).
- 768 Escada, C. (2019) Post-Rift Magmatism on the Central West Iberian Margin (Estremadura
769 Spur): New Evidences from Potential Field Data, Universidade de Lisboa.
- 770 Escada, C., Santos, F., Represas, P., Pereira, R., Mata, J., Rosas, F. & Silva, B. (2019). *Post-*
771 *Rift Magmatism on the Central West Iberian Margin: New Evidence from Magnetic and*
772 *Gravimetric Data Inversion in the Estremadura Spur*. EGU General Assembly 2019,
773 Vienna, Austria, Geophysical Research Abstracts.

774 Ferreira, E. (2017) Caracterização De Fluidos Hidrotermais E Suas Fontes Em Bacias
775 Sedimentares Com Potencial Petrolífero: Aplicação Inovadora De Análises Isotópicas Na
776 Exploração De Petróleo E Gás, Universidade de São Paulo.

777 Franke, D. (2013) Rifting, Lithosphere Breakup and Volcanism: Comparison of Magma-Poor
778 and Volcanic Rifted Margins. *Marine and Petroleum Geology*, **43**, 63-87.

779 Geoffroy, L. (2005) Volcanic Passive Margins. *Comptes Rendus Geoscience*, **337**, 1395-
780 1408. 10.1016/j.crte.2005.10.006.

781 Gpep (1986) The Petroleum Potential of Portugal, Gabinete para a Pesquisa e Exploração de
782 Petróleo. Lisboa, 62.

783 Grange, M., Schärer, U., Cornen, G. & Girardeau, J. (2008) First Alkaline Magmatism During
784 Iberia–Newfoundland Rifting. *Terra Nova*, **20**, 494-503. 10.1111/j.1365-
785 3121.2008.00847.x.

786 Grange, M., Scharer, U., Merle, R., Girardeau, J. & Cornen, G. (2010) Plume–Lithosphere
787 Interaction During Migration of Cretaceous Alkaline Magmatism in Sw Portugal: Evidence
788 from U–Pb Ages and Pb–Sr–Hf Isotopes. *Journal of Petrology*, **51**, 1143-1170.
789 10.1093/petrology/egq018.

790 Grosse, P., De Vries, B.V., Euillades, P.A., Kervyn, M. & Petrinovic, I.A. (2012) Systematic
791 Morphometric Characterization of Volcanic Edifices Using Digital Elevation Models.
792 *Geomorphology*, **136**, 114-131. 10.1016/j.geomorph.2011.06.001.

793 Grosse, P., Euillades, P.A., Euillades, L.D. & Van Wyk De Vries, B. (2013) A Global Database
794 of Composite Volcano Morphometry. *Bulletin of Volcanology*, **76**, 1-16. 10.1007/s00445-
795 013-0784-4.

796 Hubbard, R.J., Pape, J. & Roberts, D.G. (1985) Depositional Sequence Stratigraphy Mapping
797 to Illustrate the Evolution of a Passive Continental Margin. In: *Seismic Stratigraphy II: An
798 Integrated Approach* (Ed. by O. R. Berg & D. Woolverton), **39**, 93-115. AAPG, Tulsa,
799 Oklahoma.

800 Huismans, R.S., Podladchikov, Y.Y. & Cloetingh, S. (2001) Transition from Passive to Active
801 Rifting: Relative Importance of Asthenospheric Doming and Passive Extension of the
802 Lithosphere. *Journal of Geophysical Research: Solid Earth*, **106**, 11271-11291.
803 10.1029/2000jb900424.

804 Jackson, C., Magee, C. & Jacquemyn, C. (2020) Rift-Related Magmatism Influences
805 Petroleum System Development in the Ne Irish Rockall Basin, Offshore Ireland. *Petroleum
806 Geoscience*, **26**, 511-524. 10.1144/petgeo2018-020.

807 Jackson, C.a.L., Schofield, N. & Golenkov, B. (2013) Geometry and Controls on the
808 Development of Igneous Sill-Related Forced Folds: A 2-D Seismic Reflection Case Study
809 from Offshore Southern Australia. *Geological Society of America Bulletin*, **125**, 1874-1890.
810 10.1130/b30833.1.

811 Kereszturi, Á., Hargitai, H. & Zimbelman, J. (2015) Lava Flow. In: *Encyclopedia of Planetary
812 Landforms* (Ed. by H. Hargitai & Á. Kereszturi). Springer, New York, U.S.A.

813 Kullberg, J.C. & Kullberg, M.C. (2017) The Tectono-Stratigraphic Evolution of an Atlantic-Type
814 Basin: An Example from the Arrábida Sector of the Lusitanian Basin. *Ciências da Terra -
815 Earth Sciences Journal*, **19**, 55-74. 10.21695/cterra/esj.v19i1.354.

816 Leroy, M., Gueydan, F. & Dauteuil, O. (2008) Uplift and Strength Evolution of Passive Margins
817 Inferred from 2-D Conductive Modelling. *Geophysical Journal International*, **172**, 464-476.
818 10.1111/j.1365-246X.2007.03566.x.

819 Magee, C., Hunt-Stewart, E. & Jackson, C.a.L. (2013) Volcano Growth Mechanisms and the
820 Role of Sub-Volcanic Intrusions: Insights from 2d Seismic Reflection Data. *Earth and
821 Planetary Science Letters*, **373**, 41-53. <https://doi.org/10.1016/j.epsl.2013.04.041>.

822 Magee, C., Maharaj, S.M., Wrona, T. & Jackson, C.a.L. (2015) Controls on the Expression of
823 Igneous Intrusions in Seismic Reflection Data. *Geosphere*, **11**, 1024-1041.
824 10.1130/ges01150.1.

825 Magee, C., Jackson, C.a.-L., Hardman, J.P. & Reeve, M.T. (2017) Decoding Sill Emplacement
826 and Forced Fold Growth in the Exmouth Sub-Basin, Offshore Northwest Australia:
827 Implications for Hydrocarbon Exploration. *Interpretation*, **5**, SK11-SK22. 10.1190/int-2016-
828 0133.1.

829 Manatschal, G. (2004) New Models for Evolution of Magma-Poor Rifted Margins Based on a
830 Review of Data and Concepts from West Iberia and the Alps. *International Journal of Earth*
831 *Sciences*, **93**, 432-466. 10.1007/s00531-004-0394-7.

832 Manupella, G., Ferreira, A.B., Diniz, J., Callapez, P., Ribeiro, M.L., Pais, J., Rebêlo, L., Cabral,
833 J., Moniz, C., Baptista, R., Henriques, P., Falé, P., Lourenço, C., Sampaio, J., Midões, C.
834 & Zbyszewski, G. (2011) *Notícia Explicativa Da Carta Geológica 34-B, Loures, 1:50.000*.
835 Laboratório Nacional de Energia e Geologia, Lisboa. 57

836 Mark, N.J., Schofield, N., Pugliese, S., Watson, D., Holford, S., Muirhead, D., Brown, R. &
837 Healy, D. (2018) Igneous Intrusions in the Faroe Shetland Basin and Their Implications for
838 Hydrocarbon Exploration; New Insights from Well and Seismic Data. *Marine and*
839 *Petroleum Geology*, **92**, 733-753. <https://doi.org/10.1016/j.marpetgeo.2017.12.005>.

840 Marques, F.O., Azerêdo, A.C., Cabral, M.C. & Santos, V. (1998). *Preliminary Study of a*
841 *Proposed New Cartographic Unit in the Lisbon Region: The Fanhões Conglomerates*. V
842 Congresso Nacional de Geologia, Lisbon, Instituto Geológico e Mineiro.

843 Martín-Chivelet, J., Floquet, M., García-Senz, J., Callapez, P.M., López-Mir, B., Muñoz, J.A.,
844 Barroso-Barcenilla, F., Segura, M., Soares, A.F., Dinis, P.M., Marques, J.F. & Arbués, P.
845 (2019) Late Cretaceous Post-Rift to Convergence in Iberia. In: *The Geology of Iberia: A*
846 *Geodynamic Approach* (Ed. by, *Regional Geology Reviews*, **3**, 285-376. Springer.

847 Martins, L.T., Madeira, J., Youbi, N., Munhá, J., Mata, J. & Kerrich, R. (2008) Rift-Related
848 Magmatism of the Central Atlantic Magmatic Province in Algarve, Southern Portugal.
849 *Lithos*, **101**, 102–124.

850 Mata, J., Alves, C.F., Martins, L., Miranda, R., Madeira, J., Pimentel, N., Martins, S., Azevedo,
851 M.R., Youbi, N., De Min, A., Almeida, I.M., Bensalah, M.K. & Terrinha, P. (2015) ⁴⁰Ar/³⁹Ar
852 Ages and Petrogenesis of the West Iberian Margin Onshore Magmatism at the Jurassic-
853 Cretaceous Transition: Geodynamic Implications and Assessment of Open-System
854 Processes Involving Saline Materials. *Lithos*, **236-237**, 156-172.
855 <http://dx.doi.org/10.1016/j.lithos.2015.09.001>.

856 Mata, J., Martins, S., Mattielli, N., Madeira, J., Faria, B., Ramalho, R.S., Silva, P., Moreira, M.,
857 Caldeira, R., Moreira, M., Rodrigues, J. & Martins, L. (2017) The 2014–15 Eruption and
858 the Short-Term Geochemical Evolution of the Fogo Volcano (Cape Verde): Evidence for
859 Small-Scale Mantle Heterogeneity. *Lithos*, **288-289**, 91-107.
860 <https://doi.org/10.1016/j.lithos.2017.07.001>.

861 Matton, G. & Jébrak, M. (2009) The Cretaceous Peri-Atlantic Alkaline Pulse (Paap): Deep
862 Mantle Plume Origin or Shallow Lithospheric Break-Up? *Tectonophysics*, **469**, 1-12.
863 <https://doi.org/10.1016/j.tecto.2009.01.001>.

864 Mclean, C.E., Schofield, N., Brown, D.J., Jolley, D.W. & Reid, A. (2017) 3d Seismic Imaging
865 of the Shallow Plumbing System beneath the Ben Nevis Monogenetic Volcanic Field:
866 Faroe–Shetland Basin. *Journal of the Geological Society*, **174**, 468-485. 10.1144/jgs2016-
867 118.

868 Merle, R., Jourdan, F. & Girardeau, J. (2018) Geochronology of the Tore-Madeira Rise
869 Seamounts and Surrounding Areas: A Review. *Australian Journal of Earth Sciences*, **65**,
870 591-605. 10.1080/08120099.2018.1471005.

871 Merle, R.E., Jourdan, F., Chiaradia, M., Olierook, H.K.H. & Manatschal, G. (2019) Origin of
872 Widespread Cretaceous Alkaline Magmatism in the Central Atlantic: A Single Melting
873 Anomaly? *Lithos*, **342-343**, 480-498. <https://doi.org/10.1016/j.lithos.2019.06.002>.

874 Miranda, R., Valadares, V., Terrinha, P., Mata, J., Azevedo, M.D.R., Gaspar, M., Kullberg,
875 J.C. & Ribeiro, C. (2009) Age Constrains on the Late Cretaceous Alkaline Magmatism on
876 the West Iberian Margin. *Cretaceous Research*, **30**, 575-586.

877 Miranda, R. (2010) Petrogenesis and Geochronology of the Late Cretaceous Alkaline
878 Magmatism in the West Iberian Margin, Universidade de Lisboa, Lisboa.

879 Miranda, R., Terrinha, P., Mata, J., Azevedo, M.D.R., Chadwick, J., Lourenço, N. & Moreira,
880 M. (2010). *Caracterização Geoquímica Do Monte Submarino De Fontanelas, Margem*
881 *Oeste Ibérica*. X Congresso de geoquímica dos países de língua oficial portuguesa, XVI
882 Semana de geoquímica, Porto, Portugal, Universidade do Porto.

883 Neres, M., Bouchez, J.L., Terrinha, P., Font, E., Moreira, M., Miranda, R., Launeau, P. &
884 Carvalho, C. (2014) Magnetic Fabric in a Cretaceous Sill (Foz Da Fonte, Portugal): Flow
885 Model and Implications for Regional Magmatism. *Geophysical Journal International*, **199**,
886 78-101. 10.1093/gji/ggu250.

887 Neres, M., Terrinha, P., Custódio, S., Silva, S.M., Luis, J. & Miranda, J.M. (2018) Geophysical
888 Evidence for a Magmatic Intrusion in the Ocean-Continent Transition of the Sw Iberia
889 Margin. *Tectonophysics*, **744**, 118-133. <https://doi.org/10.1016/j.tecto.2018.06.014>.

890 Niyazi, Y., Eruteya, O.E., Warne, M. & Ierodiaconou, D. (2021a) Discovery of Large-Scale
891 Buried Volcanoes within the Cenozoic Succession of the Prawn Platform, Offshore Otway
892 Basin, Southeastern Australia. *Marine and Petroleum Geology*, **123**, 104747.
893 <https://doi.org/10.1016/j.marpetgeo.2020.104747>.

894 Niyazi, Y., Warne, M. & Ierodiaconou, D. (2021b) Post-Rift Magmatism and Hydrothermal
895 Activity in the Central Offshore Otway Basin and Implications for Igneous Plumbing
896 Systems. *Marine Geology*, **438**, 106538. <https://doi.org/10.1016/j.margeo.2021.106538>.

897 Oyarzun, R., Doblas, M., López-Ruiz, J. & María Cebra, J. (1997) Opening of the Central
898 Atlantic and Asymmetric Mantle Upwelling Phenomena: Implications for Long-Lived
899 Magmatism in Western North Africa and Europe. *Geology*, **25**, 727-730. 10.1130/0091-
900 7613(1997)025<0727:ootcaa>2.3.co;2.

901 Pereira, R., Alves, T.M. & Mata, J. (2017) Alternating Crustal Architecture in West Iberia: A
902 Review of Its Significance in the Context of Ne Atlantic Rifting. *Journal of the Geological
903 Society*, **174**, 522-540. 10.1144/jgs2016-050.

904 Pereira, R. & Barreto, P. (2018). *Evidence and Significance of Buried Magmatic Features
905 Offshore the West Iberian Margin*. AAPG Europe Conference and Exhibition, Lisbon,
906 Portugal.

907 Pereira, R., Rosas, F., Mata, J., Represas, P., Escada, C. & Silva, B. (2021) Interplay of
908 Tectonics and Magmatism During Post-Rift Inversion on the Central West Iberian Margin
909 (Estremadura Spur). *Basin Research*, **33**, 1497-1519. 10.1111/bre.12524.

910 Pérez-Gussinyé, M., Morgan, J.P., Reston, T.J. & Ranero, C.R. (2006) The Rift to Drift
911 Transition at Non-Volcanic Margins: Insights from Numerical Modelling. *Earth and
912 Planetary Science Letters*, **244**, 458-473. <https://doi.org/10.1016/j.epsl.2006.01.059>.

913 Peterson, D.W. & Tilling, R.I. (1980) Transition of Basaltic Lava from Pahoehoe to Aa, Kilauea
914 Volcano, Hawaii: Field Observations and Key Factors. *Journal of Volcanology and
915 Geothermal Research*, **7**, 271-293. [https://doi.org/10.1016/0377-0273\(80\)90033-5](https://doi.org/10.1016/0377-0273(80)90033-5).

916 Planke, S., Rasmussen, T., Rey, S.S. & Myklebust, R. (2005) Seismic Characteristics and
917 Distribution of Volcanic Intrusions and Hydrothermal Vent Complexes in the Vøring and
918 Møre Basins. *Geological Society, London, Petroleum Geology Conference series*, **6**, 833-
919 844. 10.1144/0060833.

920 Planke, S., Svensen, H., Myklebust, R., Bannister, S., Manton, B. & Lorenz, L. (2015)
921 Geophysics and Remote Sensing. In: *Physical Geology of Shallow Magmatic Systems*
922 (Ed. by, 131-146.

923 Planke, S., Millett, J.M., Maharjan, D., Jerram, D.A., Abdelmalak, M.M., Groth, A., Hoffmann,
924 J., Berndt, C. & Myklebust, R. (2017) Igneous Seismic Geomorphology of Buried Lava
925 Fields and Coastal Escarpments on the Vøring Volcanic Rifted Margin. *Interpretation*, **5**,
926 SK161-SK177. 10.1190/int-2016-0164.1.

927 Pyle, D.M. (2015) Sizes of Volcanic Eruptions, in Sigurdsson, H., Houghton, B., McNutt, S.,
928 Rymer, H. And Stix, J. Eds., 2000. The Encyclopedia of Volcanoes. Academic Press. In:
929 *The Encyclopedia of Volcanoes* (Ed. by H. Sigurdsson), 257-264. Elsevier.

930 Ramalho, M.M., Pais, J., Rey, J., Berthou, P.-Y., Alves, C.a.M., Palacios, T., Leal, N. &
931 Kullberg, M.C. (1993) Notícia Explicativa Da Folha 34-a, Sintra, 1:50000. S. G. d. Portugal,
932 77.

933 Rey, J., Dinis, J.L., Callapez, P. & Cunha, P.P. (2006) *Da Rotura Continental À Margem
934 Passiva: Composição E Evolução Do Cretácico De Portugal*. INETI, Lisboa, Portugal. 75

935 Reynolds, P., Holford, S., Schofield, N. & Ross, A. (2017a) The Shallow Depth Emplacement
936 of Mafic Intrusions on a Magma-Poor Rifted Margin: An Example from the Bight Basin,

937 Southern Australia. *Marine and Petroleum Geology*, **88**, 605-616.
938 <https://doi.org/10.1016/j.marpetgeo.2017.09.008>.

939 Reynolds, P., Holford, S., Schofield, N. & Ross, A. (2017b) Three-Dimensional Seismic
940 Imaging of Ancient Submarine Lava Flows: An Example from the Southern Australian
941 Margin. *Geochemistry, Geophysics, Geosystems*, **18**, 3840-3853.
942 <https://doi.org/10.1002/2017GC007178>.

943 Rock, N.M.S. (1982) The Late Cretaceous Alkaline Igneous Province in the Iberian Peninsula,
944 and Its Tectonic Significance. *Lithos*, **15**, 111-131. [https://doi.org/10.1016/0024-4937\(82\)90004-4](https://doi.org/10.1016/0024-4937(82)90004-4).

946 Schofield, N.J., Brown, D.J., Magee, C. & Stevenson, C.T. (2012) Sill Morphology and
947 Comparison of Brittle and Non-Brittle Emplacement Mechanisms. *Journal of the
948 Geological Society*, **169**, 127-141. 10.1144/0016-76492011-078.

949 Senger, K., Millett, J., Planke, S., Ogata, K., Haug Eide, C., Festøy, M., Galland, O. & Jerram,
950 D.A. (2017) Effects of Igneous Intrusions on the Petroleum System: A Review. *First Break*,
951 **35**. <https://doi.org/10.3997/1365-2397.2017011>.

952 Sheridan, M.F. & Wohletz, K.H. (1981) Hydrovolcanic Explosions: The Systematics of Water-
953 Pyroclast Equilibration. *Science*, **212**, 1387-1389. doi:10.1126/science.212.4501.1387.

954 Silva, E.A., Miranda, J.M., Luis, J.F. & Galdeano, A. (2000) Correlation between the
955 Palaeozoic Structures from West Iberian and Grand Banks Margins Using Inversion of
956 Magnetic Anomalies. *Tectonophysics*, **321**, 57-71. [https://doi.org/10.1016/S0040-1951\(00\)00080-9](https://doi.org/10.1016/S0040-1951(00)00080-9).

958 Silva, S.D. & Lindsay, J.M. (2015) Primary Volcanic Landforms. In: *The Encyclopedia of
959 Volcanoes* (Ed. by H. Sigurdsson), 273-297.

960 Simões, P., Neres, M. & Terrinha, P. (2020). *Joint Modeling of Seismic, Magnetic and
961 Gravimetric Data Unravels the Extent of the Late Cretaceous Magmatic Province on the
962 Estremadura Spur Offshore West Iberia*. EGU General Assembly.

963 Smallwood, J.R. & Maresh, J. (2002) The Properties, Morphology and Distribution of Igneous
964 Sills: Modelling, Borehole Data and 3d Seismic from the Faroe-Shetland Area. *Geological
965 Society, London, Special Publications*, **197**, 271-306. 10.1144/gsl.Sp.2002.197.01.11.

966 Sohn, Y.K. (1996) Hydrovolcanic Processes Forming Basaltic Tuff Rings and Cones on Cheju
967 Island, Korea. *GSA Bulletin*, **108**, 1199-1211.

968 Sparks, R.S.J. & Wadge, G. (1975) Geological and Geochemical Studies of the Sintra Alkaline
969 Igneous Complex, Portugal. *Bulletin Volcanologique*, **39**, 385-406. 10.1007/BF02597263.

970 Sun, Q., Jackson, C.a.L., Magee, C., Mitchell, S.J. & Xie, X. (2019) Extrusion Dynamics of
971 Deepwater Volcanoes Revealed by 3-D Seismic Data. *Solid Earth*, **10**, 1269-1282.
972 10.5194/se-10-1269-2019.

973 Sun, Q., Magee, C., Jackson, C.a.L., Mitchell, S.J. & Xie, X. (2020) How Do Deep-Water
974 Volcanoes Grow? *Earth and Planetary Science Letters*, **542**. 10.1016/j.epsl.2020.116320.

975 Terrinha, P., Pueyo, E.L., Aranguren, A., Kullberg, J.C., Kullberg, M.C., Casas-Sainz, A. &
976 Azevedo, M.D.R. (2017) Gravimetric and Magnetic Fabric Study of the Sintra Igneous
977 Complex: Laccolith-Plug Emplacement in the Western Iberian Passive Margin.
978 *International Journal of Earth Sciences*, **107**, 1807-1833. 10.1007/s00531-017-1573-7.

979 Thomson, K. (2004) Volcanic Features of the North Rockall Trough: Application of
980 Visualisation Techniques on 3d Seismic Reflection Data. *Bulletin of Volcanology*, **67**, 116-
981 128. 10.1007/s00445-004-0363-9.

982 Thomson, K. & Hutton, D. (2004) Geometry and Growth of Sill Complexes: Insights Using 3d
983 Seismic from the North Rockall Trough. *Bulletin of Volcanology*, **66**, 364-375.
984 10.1007/s00445-003-0320-z.

985 Verati, C., Rapaille, C., Feraud, G., Marzoli, A., Bertrand, H. & Youbi, N. (2007) Ar-40/Ar-39
986 Ages and Duration of the Central Atlantic Magmatic Province Volcanism in Morocco and
987 Portugal and Its Relation to the Triassic-Jurassic Boundary. *Palaeogeography,
988 Palaeoclimatology, Palaeoecology*, **244**, 308-325.

989 Verwoerd, W.J. & Chevallier, L. (1987) Contrasting Types of Surtseyan Tuff Cones on Marion
990 and Prince Edward Islands, Southwest Indian Ocean. *Bulletin of Volcanology*, **49**, 399-
991 413. 10.1007/BF01046633.

- 992 Walker, F., Schofield, N., Millett, J., Jolley, D., Holford, S., Planke, S., Jerram, D.A. &
993 Myklebust, R. (2020) Inside the Volcano: Three-Dimensional Magmatic Architecture of a
994 Buried Shield Volcano. *Geology*. 10.1130/g47941.1.
- 995 White, J.D.L., Mcphie, J. & Soule, S.A. (2015) Chapter 19 - Submarine Lavas and
996 Hyaloclastite. In: *The Encyclopedia of Volcanoes (Second Edition)* (Ed. by H. Sigurdsson),
997 363-375. Academic Press, Amsterdam.
- 998 Witt, W.G. (1977) Stratigraphy of the Lusitanian Basin, Shell Prospex Portuguesa, 61.
- 999 Wright, J.B. (1969) Re-Interpretation of a Mixed Petrographic Province—the Sintra Intrusive
1000 Complex (Portugal) and Related Rocks. *Geologische Rundschau*, **58**, 538-564.
- 1001 Zhao, F., Alves, T.M., Wu, S., Li, W., Huuse, M., Mi, L., Sun, Q. & Ma, B. (2016) Prolonged
1002 Post-Rift Magmatism on Highly Extended Crust of Divergent Continental Margins (Baiyun
1003 Sag, South China Sea). *Earth and Planetary Science Letters*, **445**, 79-91.
1004 <https://doi.org/10.1016/j.epsl.2016.04.001>.
- 1005
- 1006

Figures

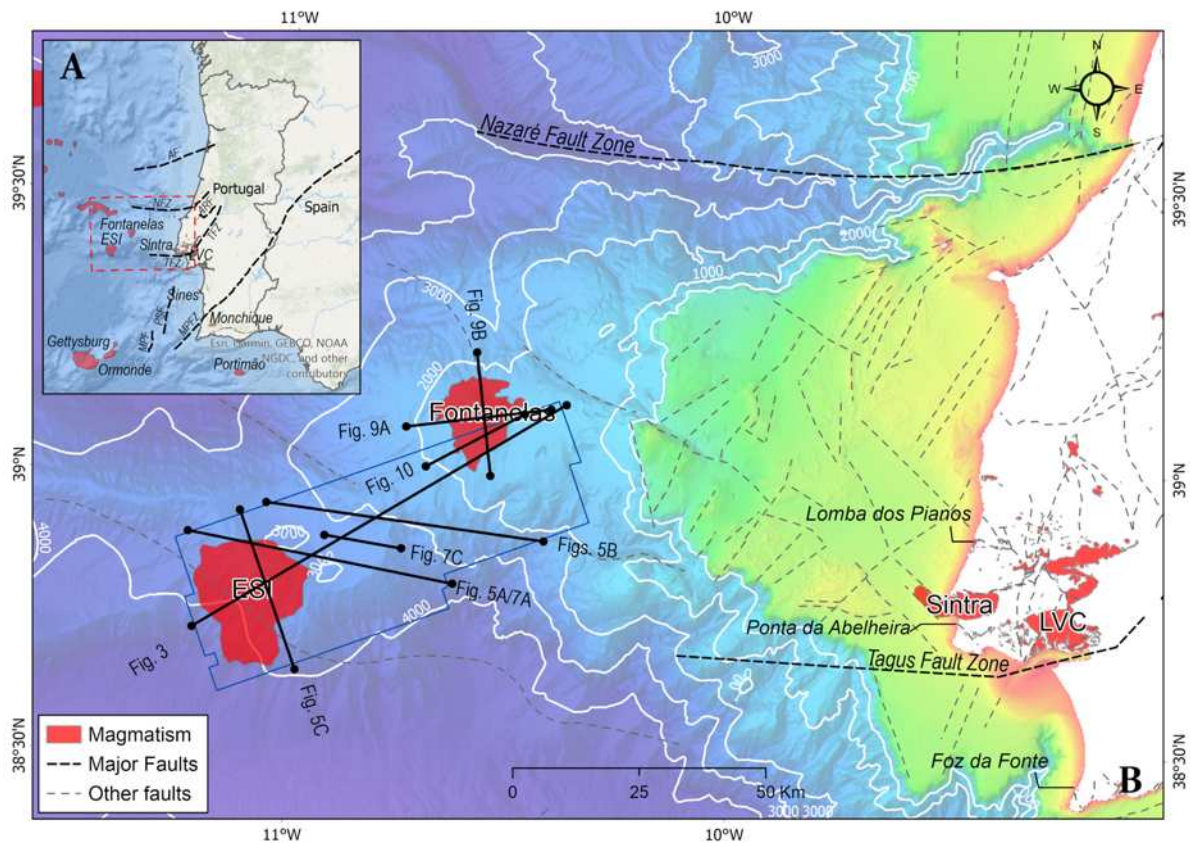


Figure 1. Location of the area of interest showing the distribution of magmatism on the central West Iberian Margin. ESI – Estremadura Spur Intrusion, LVC – Lisbon Volcanic Complex, AF – Aveiro Fault, NFZ – Nazaré Fault Zone, TFZ – Tagus Fault Zone, PSF – Pereira de Sousa Fault, MPF – Marquês de Pombal Fault, MPFZ – Messejana-Plasencia Fault Zone.

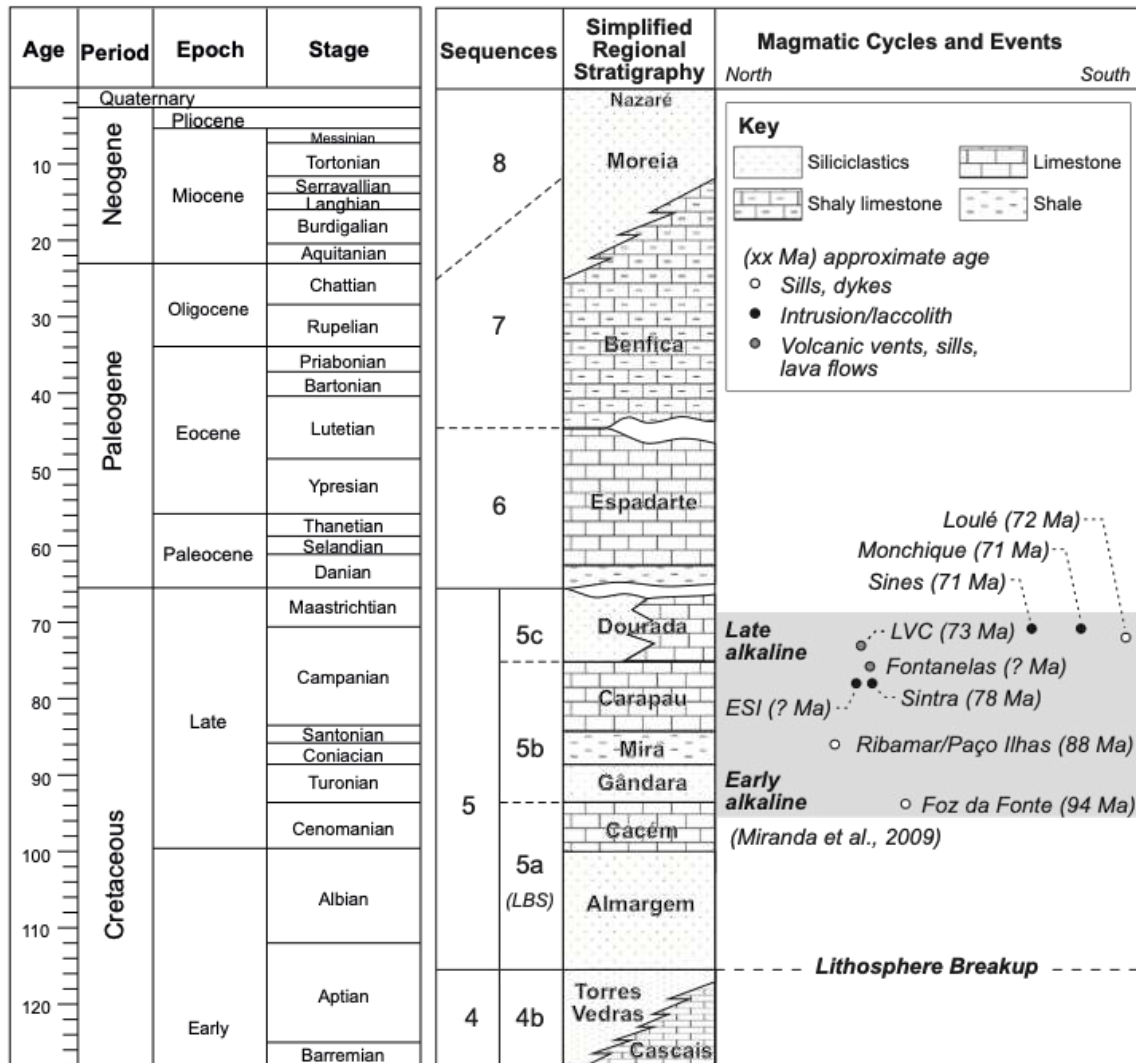


Figure 2. Stratigraphic framework of the West Iberian Margin showing the distinct megasequences, lithostratigraphic units and evidence of the Late Cretaceous alkaline magmatism. LBS – Lithosphere Breakup Sequence (Unit 5a).

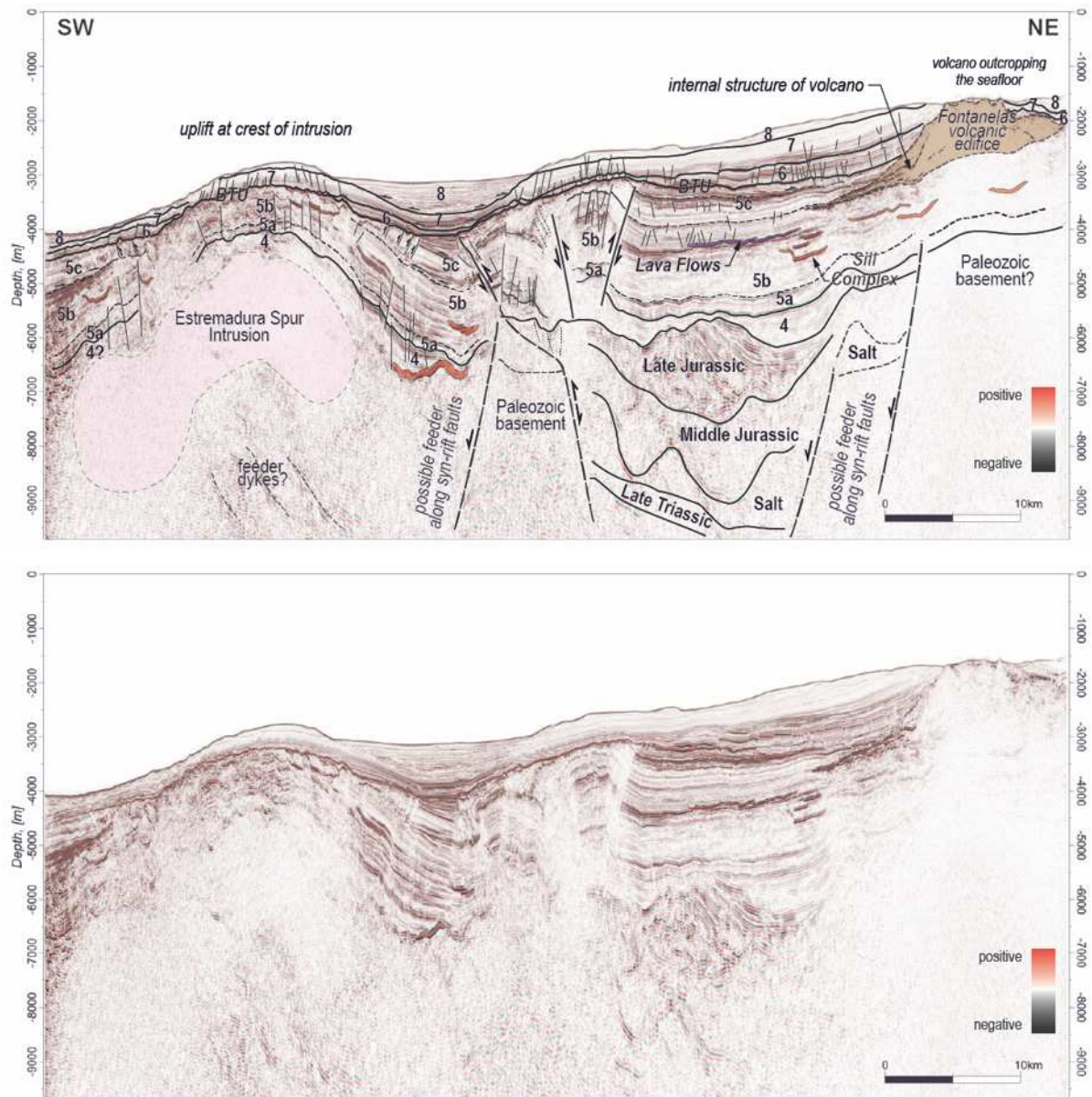


Figure 3. Seismic line (in depth) across the Estremadura Spur, showing the evidence of the Fontanelas volcano, the Estremadura Spur Intrusion with associated sills (red) and lava flows (purple), as part of the larger magmatic plumbing system of the Late Cretaceous. BTU – Base Tertiary Unconformity.

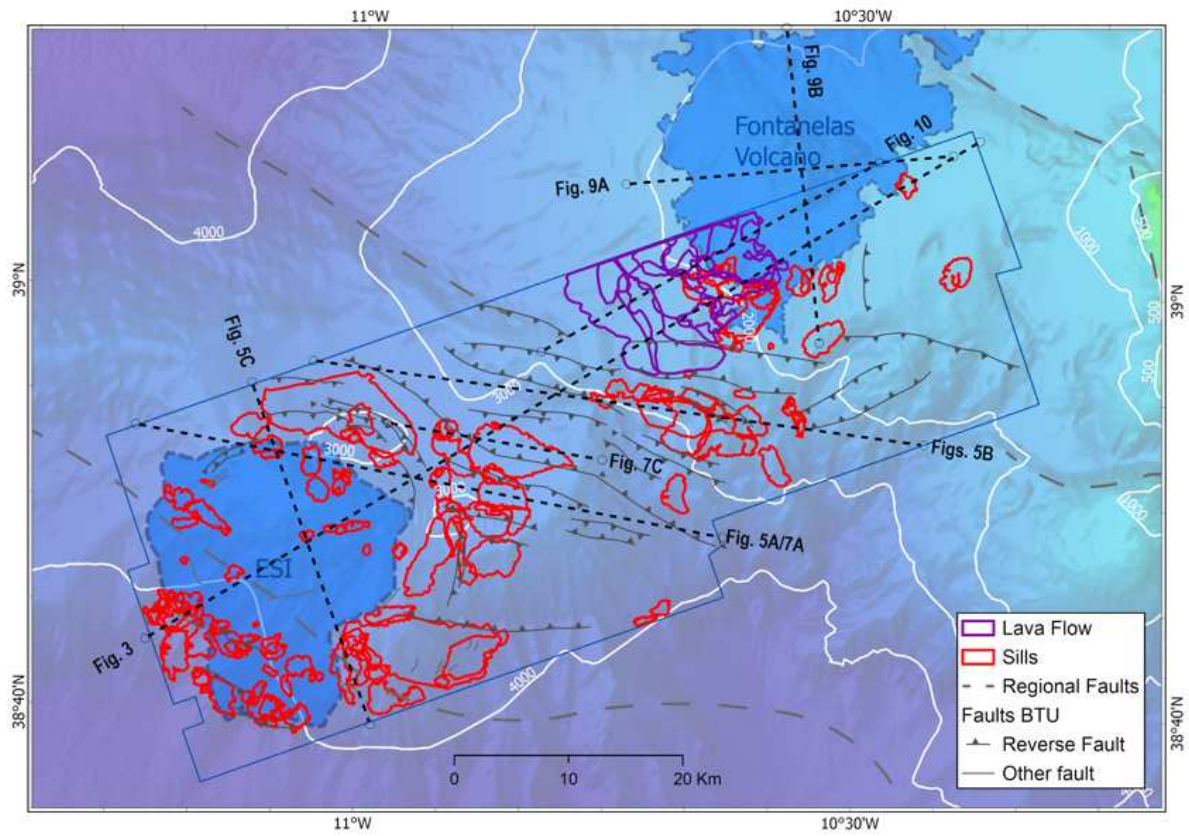
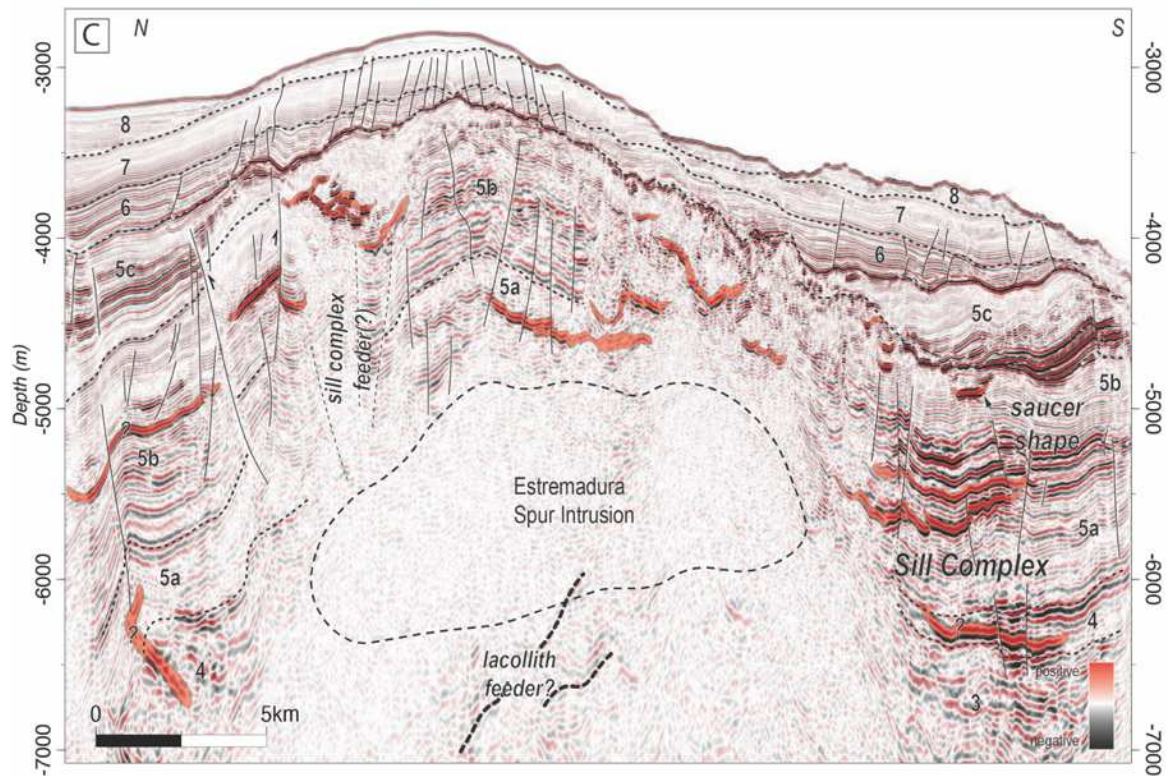
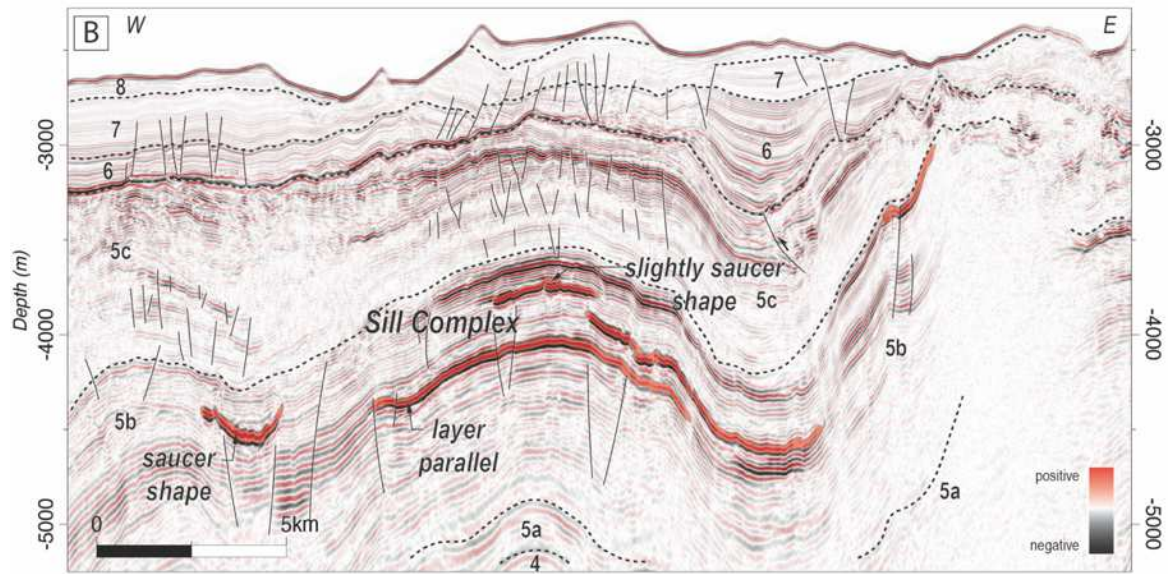
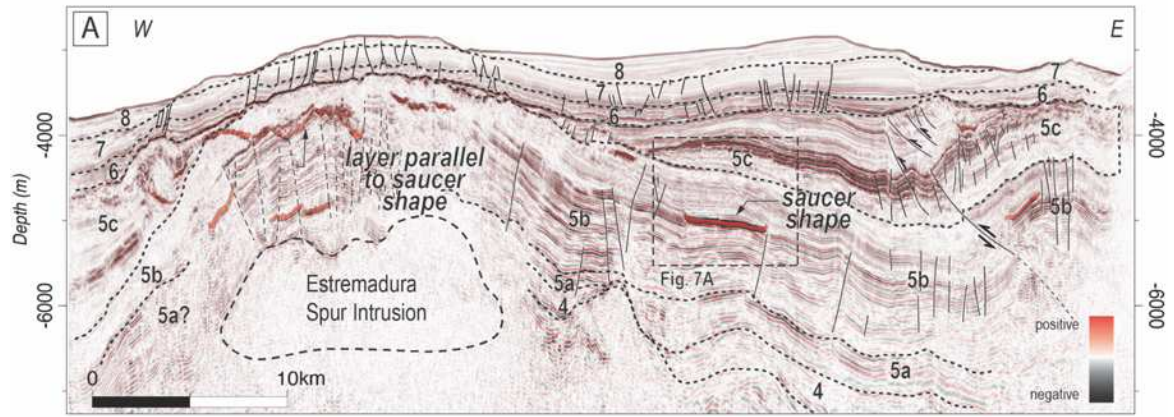


Figure 4. Map showing the location of the Estremadura Spur Intrusion (ESI), the Fontanelas volcano and the dominant distribution of sills (red) and lava flows (purple).



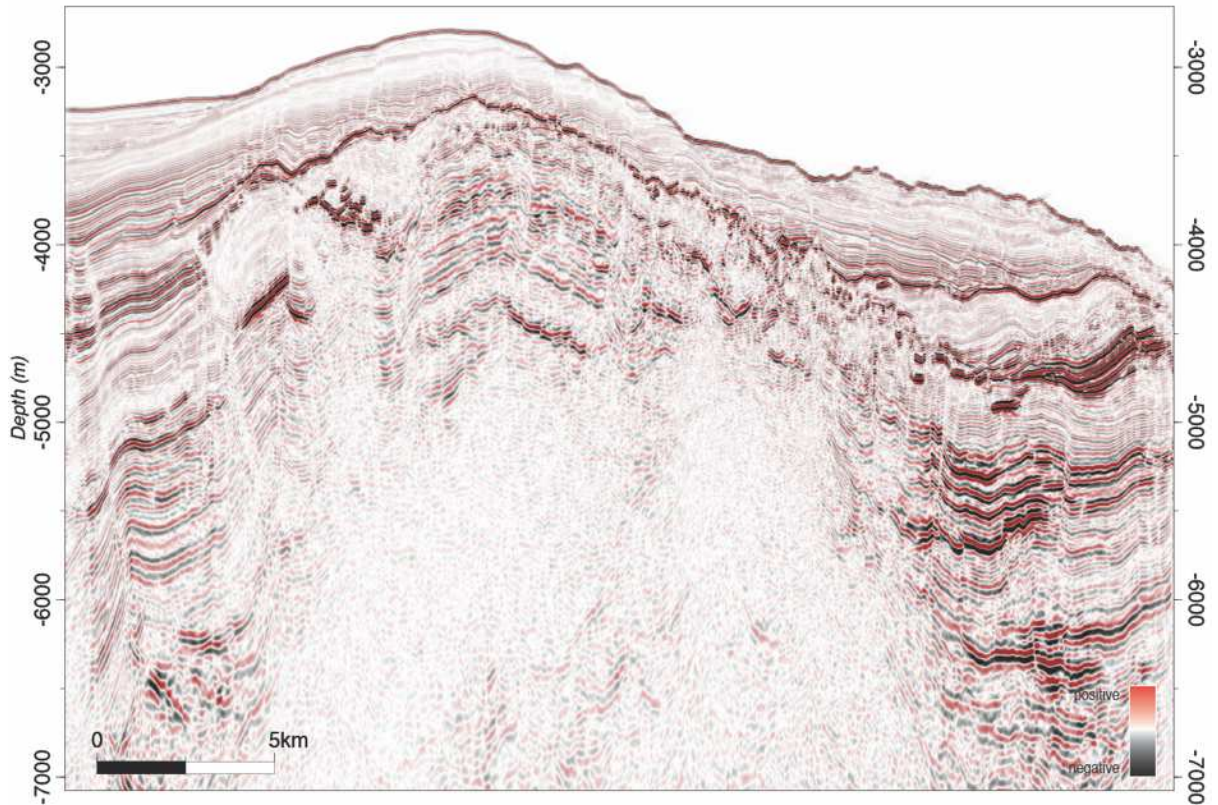
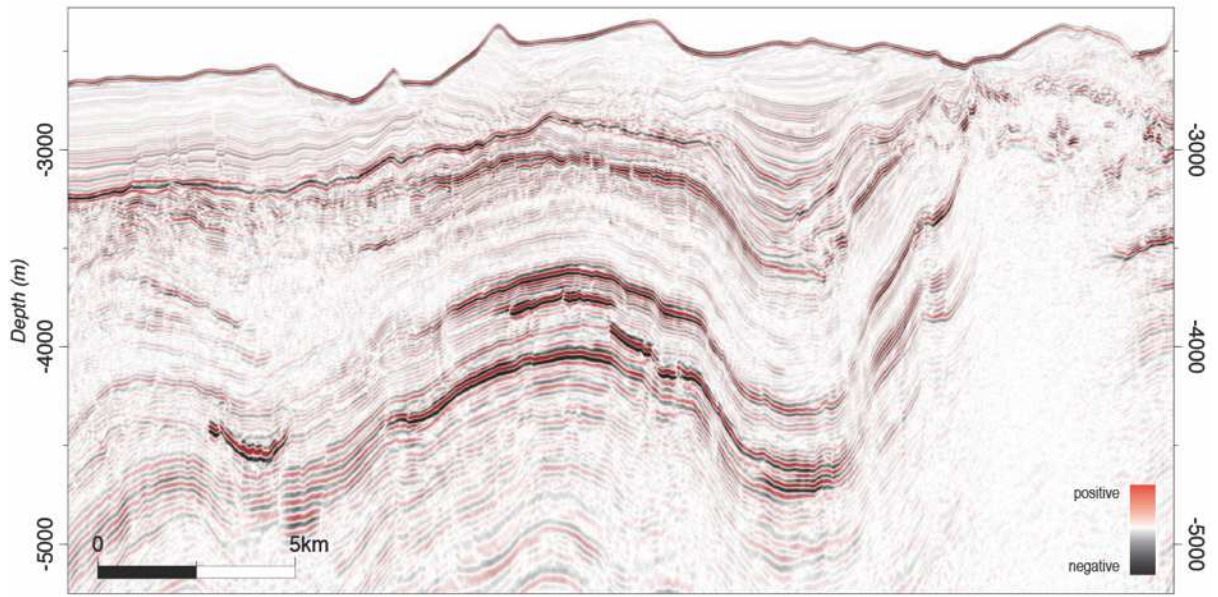
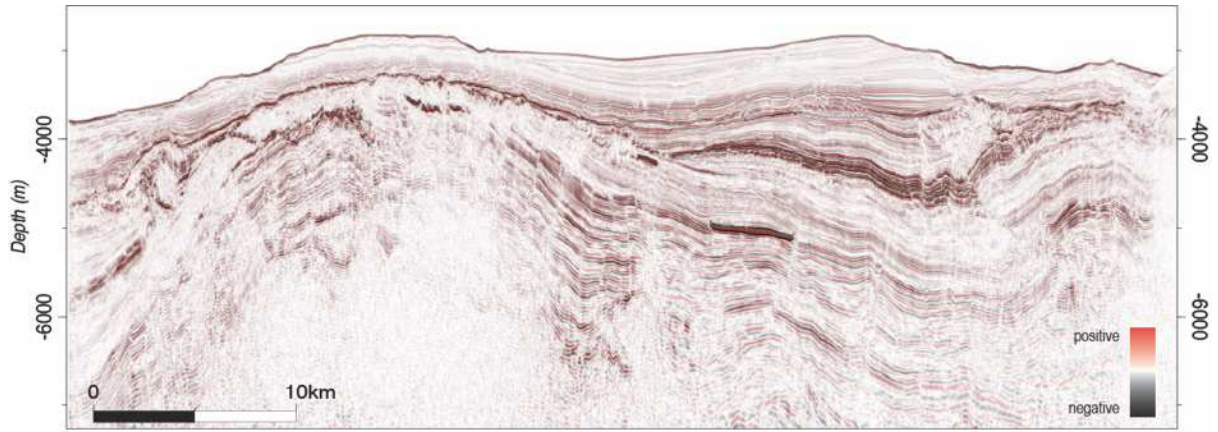


Figure 5. Seismic lines (in depth) showing the distribution and different geometry of sills (in red) throughout the Estremadura Spur. Note that sills and sill complexes are dominantly emplaced within sequence 5b. Location of seismic lines in figure 4.

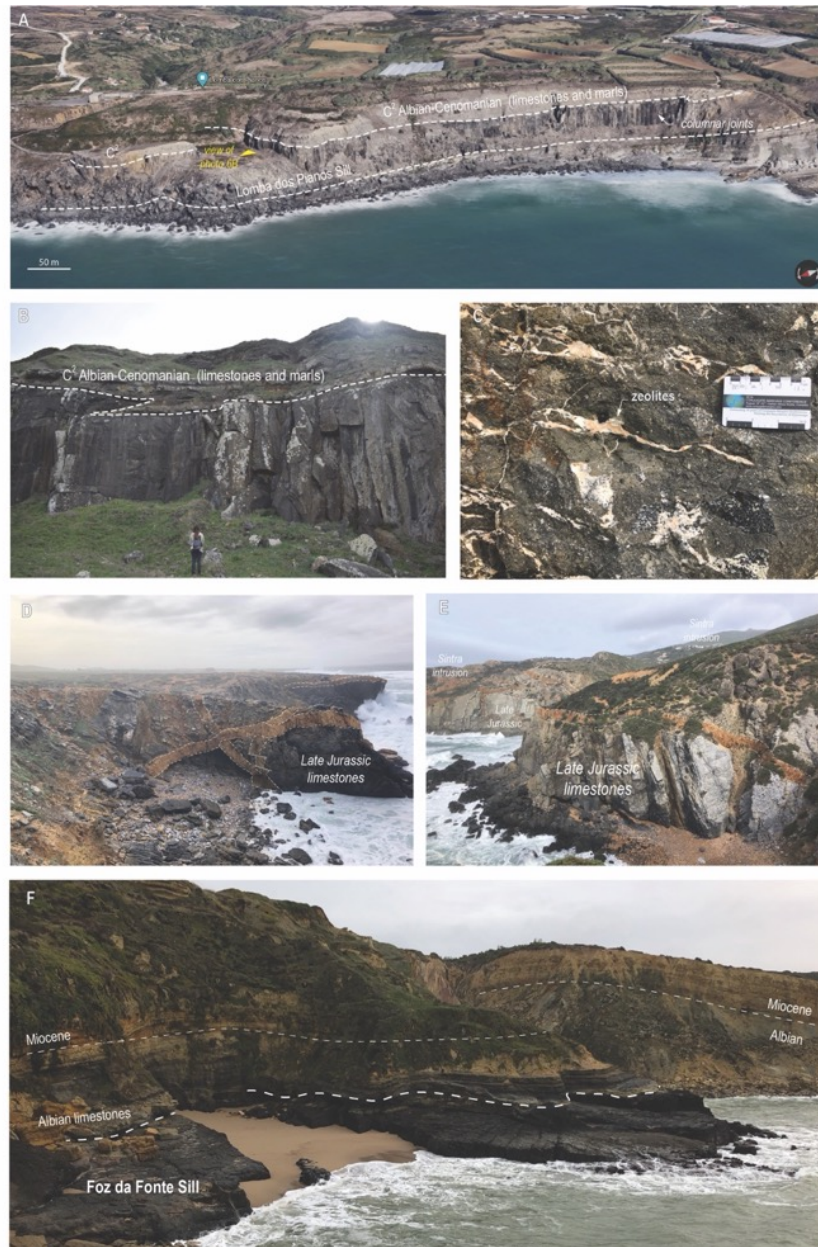


Figure 6. Outcropping examples of the Late Cretaceous magmatism. A) Lomba dos Planos sill, as seen on Google Maps perspective, showing the relation between the Albian-Cenomanian limestones and marls. Approximate thickness of the sill is 30-40 m. Lat: 38°53'36.22"N, Long: 9°26'18.00"W. B) Detail of the Lomba dos Planos sill showing the top contact with limestones, evidencing prismatic joints. View to the South. C) Detail of the basaltic sill, showing zeolites filling fractures. D) Crosscutting trachytic-basaltic(?) ring dykes associated with the Sintra intrusion, at Ponta da Abelheira. View to the South. Lat: 38°44'52.81"N; Long: 9°28'18.36"W. E) Trachytic-basaltic(?) dykes and sills crosscutting late Jurassic limestones at Ponta da Abelheira, showing the landscape of the Sintra massif at a distance. F) The Foz da Fonte sill intruding Albian limestones, an example of forced folding associated with shallow magma emplacement; Lat: 38°27'3.91"N, Long: 9°12'6.25"W.

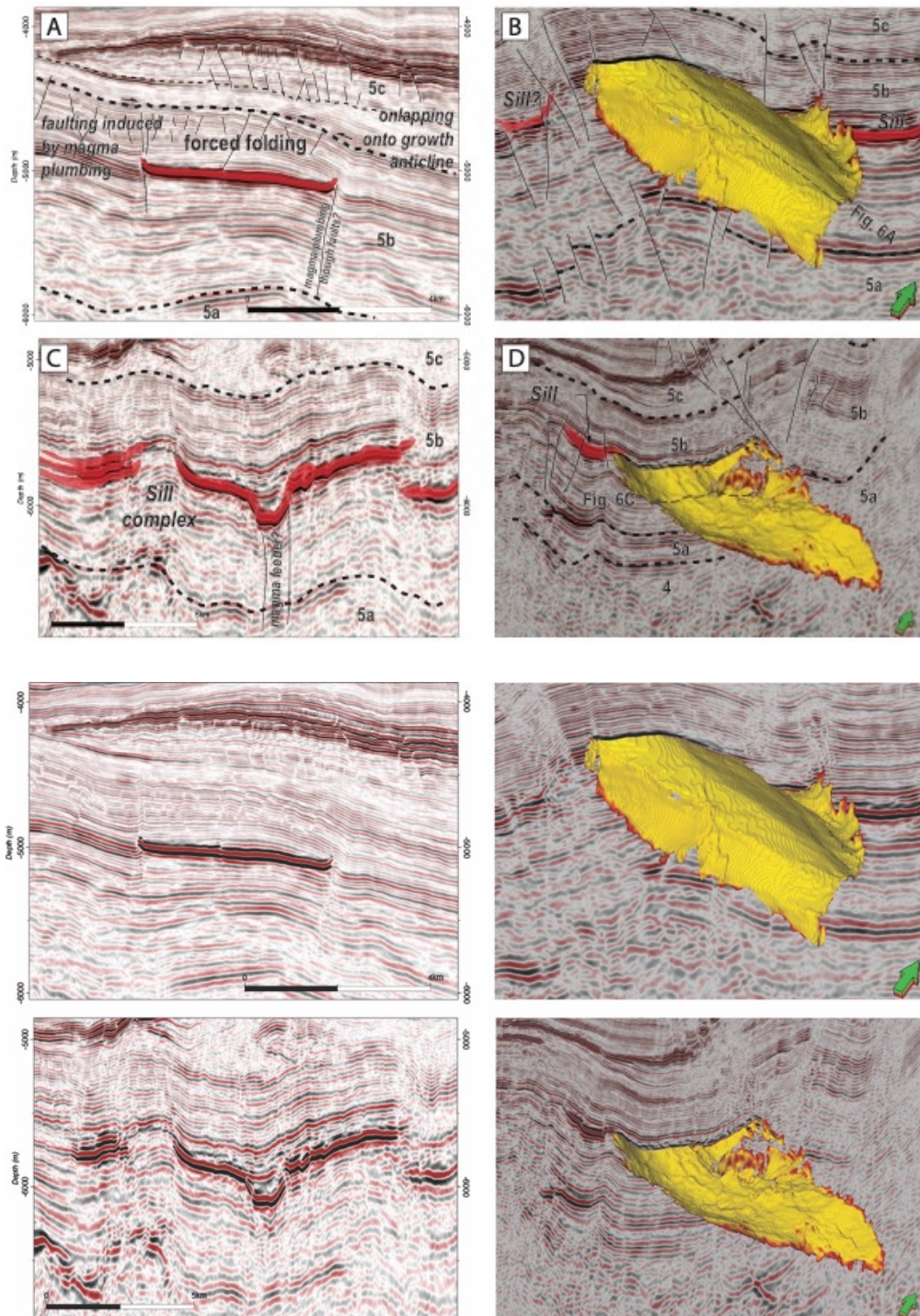


Figure 7. Details of sills intruding the Estremadura Spur. A) Seismic section showing an example of a planar-slightly saucer chape sill intruding unit 5b, with forced folding and faulting of overburden strata, with onlaps at base of sequence 5c. Note faulting at the edge of sill, tentatively interpreted as conduit for magma emplacement. B) 3D view of the sill showing the flanks of the sill. C) Sill complex intruding unit 5b, highlighting the presence of a saucer-shape sill and possible magma conduit. D) 3D view of the sill, showing its complex geometry and possible source of magma flow.

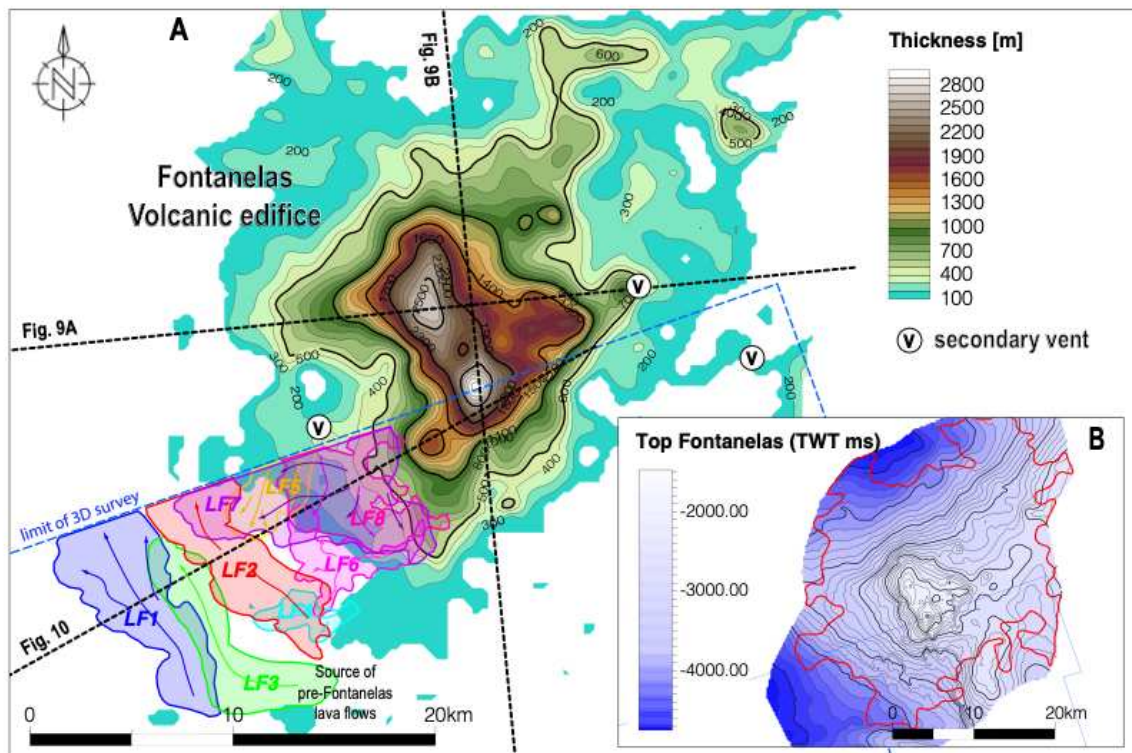
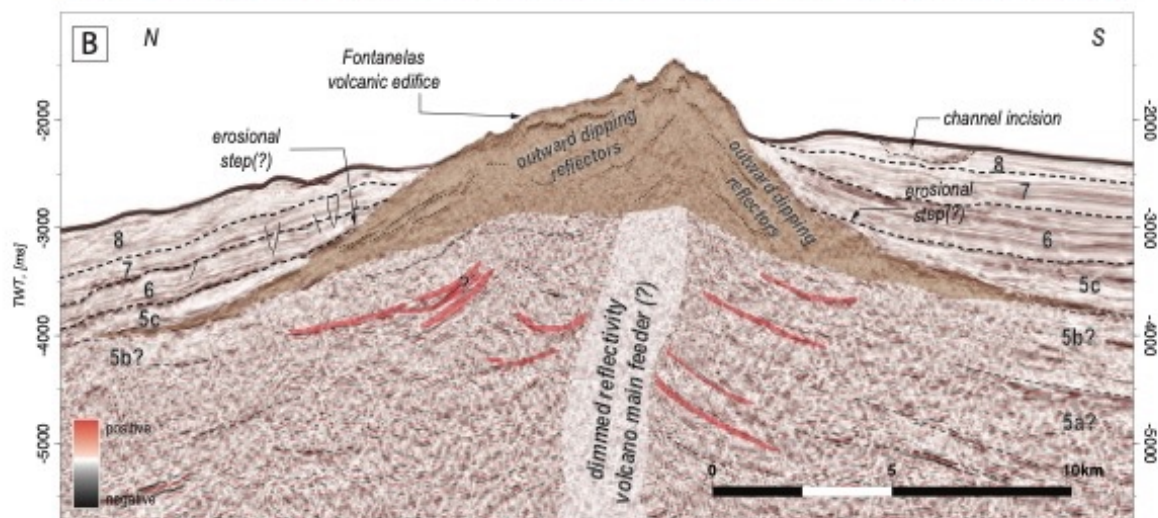
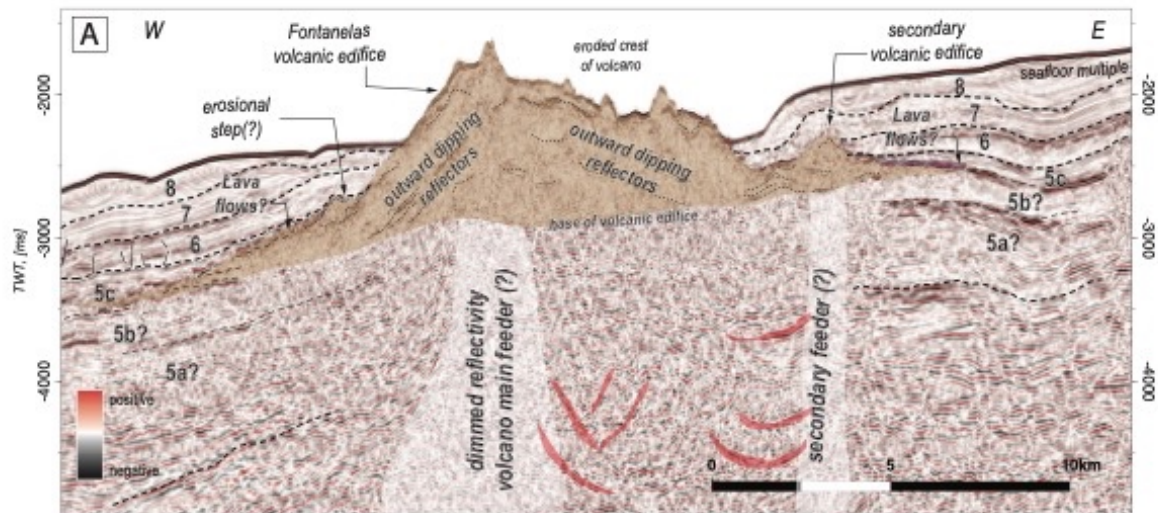


Figure 8. A) Thickness map of the Fontanelas volcanic edifice, based on 2D/3D seismic data, with associated lavas (1 to 8), with interpreted flow directions from a common source. Note the presence of secondary volcanic vents. B) TWT structural map of the Fontanelas volcano.



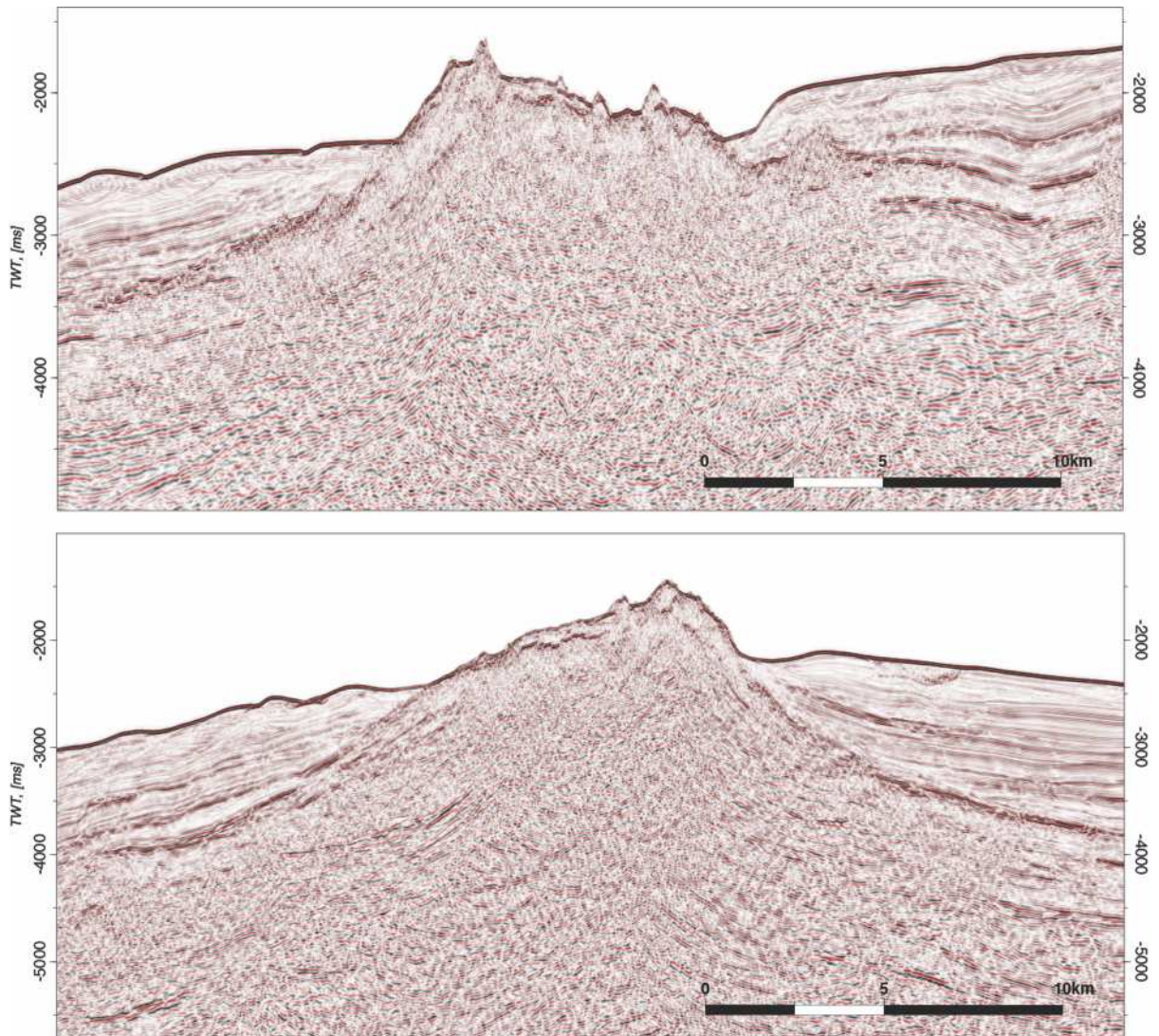


Figure 9. TWT seismic lines across the Fontanelas volcano, highlighting the internal structuration and build-up of the volcanic edifice (outward dipping reflectors), lava flows (in purple), associated secondary vents and deep plumbing systems with multiple sills (in red). Possible erosional terraces at the flank of the volcano suggest possible influence of submergence and shallow water conditions.

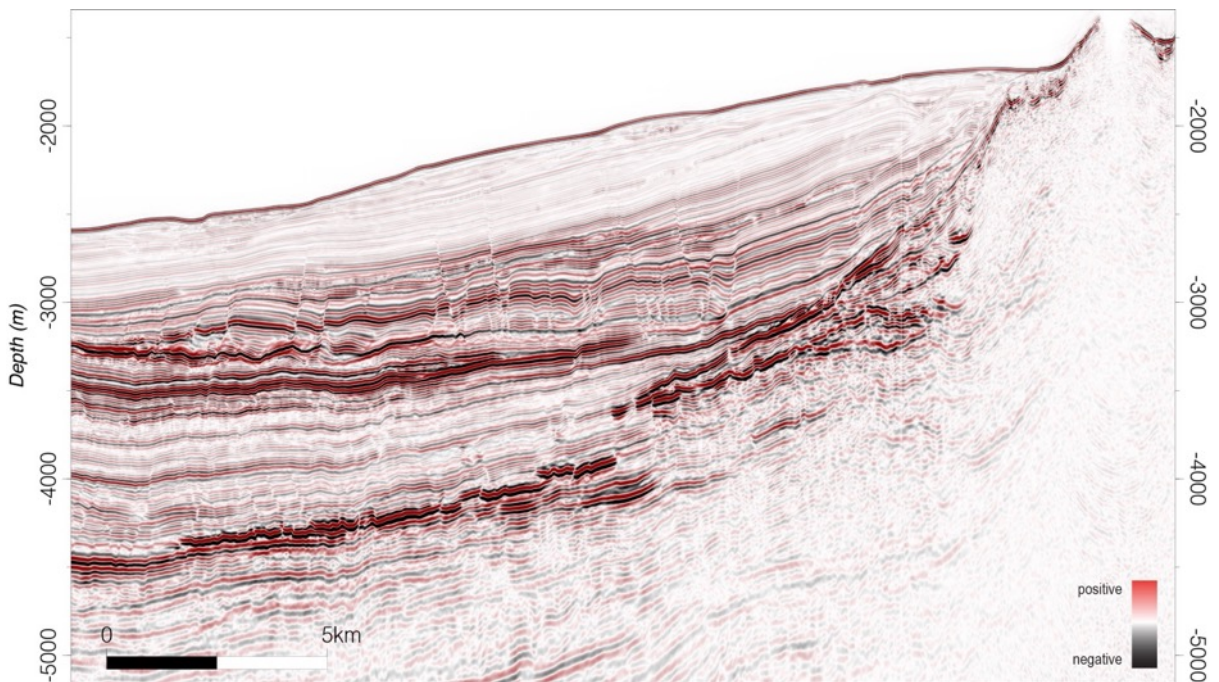
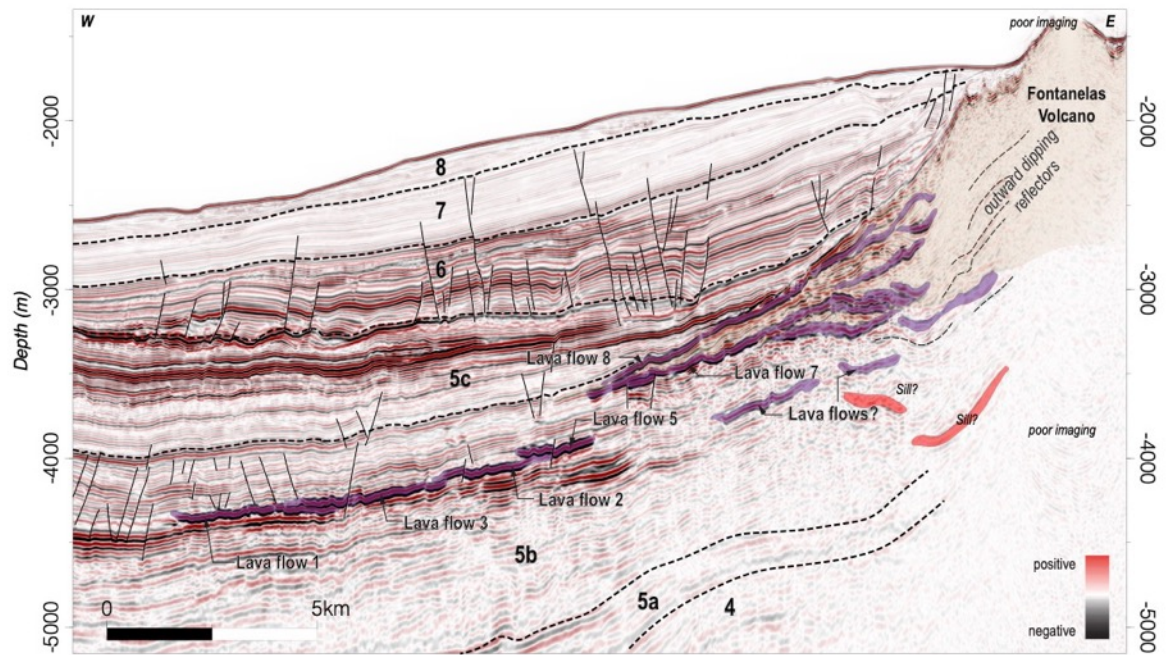


Figure 10. Random seismic line across the southern flank of the volcano, showing pre-Fontanelas lava flows (1 to 5) and syn-Fontanelas lava flows (6-8). See figure 8 for location, figure 11 and Table 1 for details of the lava flows.

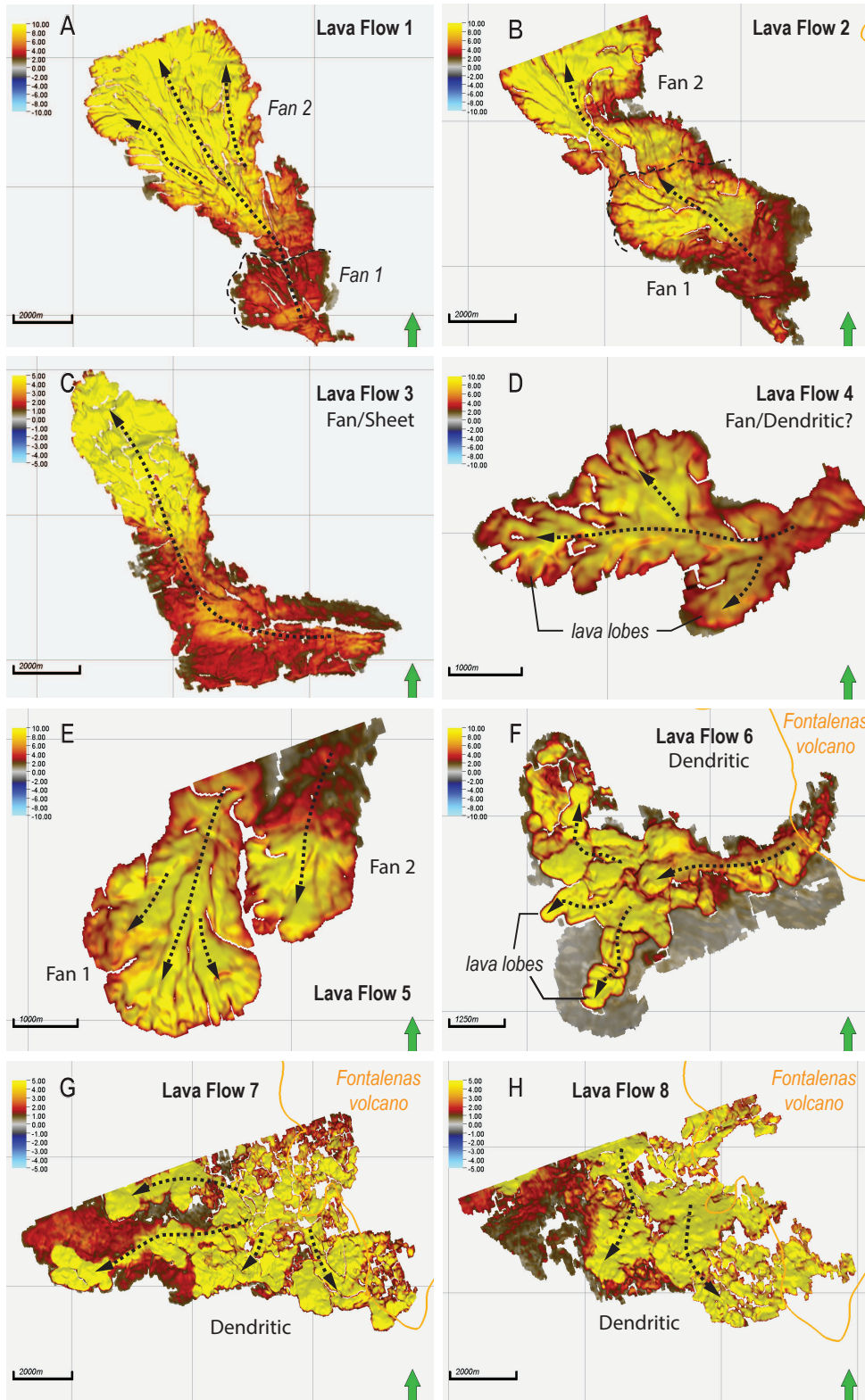


Figure 11. Plan view of seismic amplitudes of interpreted flows, showing multiple lava fans, lobate to crenulated terminations. Arrows indicate likely direction of flow, in relation to its interpreted source and the position of the Fontanelas volcano.

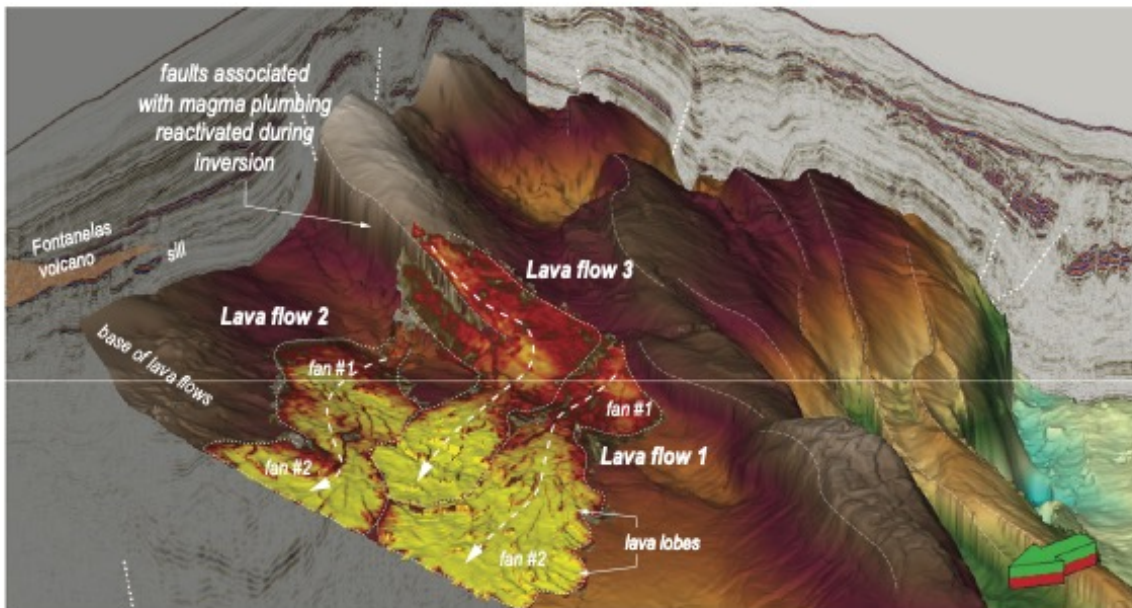


Figure 12. 3D perspective (in depth) of pre-Fontanelas lava flows and interpreted source for fissural magmatism preceding the build-up of the main volcanic edifice. Note the confluence of the origin of lava flows onto inversion faults, likely inherited from the syn-rift architecture.

Nr	Description	Main Direction of Flow	Area (Km²)	Rock Volume (km³)	Sequence	Relative age
LF1	Lava fans with coalesced lobes	Northwest	37.6	0,87	5b	Pre-Fontanelas
LF2	Lava fans	Northwest	31.1	0,54	5b	Pre-Fontanelas
LF3	Lava sheet/fan(?).	Northwest	28.8	0,95	5b	Pre-Fontanelas
LF4	Possible lava fan with splays and lobes	West	6.8	0,14	5b	Pre-Fontanelas
LF5	Lava fans showing multiple coalesced lobes	South	11.4	0,19	5b	Pre-Fontanelas
LF6	Formed by individual channels of lava, with an overall dendritic shape and individual lobes	West	13.7	0,18	5c	Base Fontanelas
LF7	Multiple dendritic lava flows	South/Southwest	46.1	0,69	5c	Base Fontanelas
LF8	Dendritic lava flows	South	26.6	0,20	5c	Intra-Fontanelas